

Chapter 1

Introduction

1.1 Dense WDM system

A communication system transmits information from one place to another, whether separated by a few kilometers or by transoceanic distance. Information is often carried by an electromagnetic carrier wave whose frequency can vary from a few mega-hertz to several hundred tera-hertz. Optical communication use high carrier frequency (~ 100 THz) in the visible or near-infrared region of the electromagnetic spectrum. They are sometimes called lightwave system to distinguish them from microwave system.

In principle, the capacity of optical communication system can exceed 10 Tb/s because of large frequency associated with the optical carrier. In practice however, the bit rate was limit to 10 Gb/s or less until 1995 because of the limitations imposed by the dispersive and nonlinear effects and by the speed of electronic components. Since then, transmission of multiple optical channels over the same fiber has provided a simple way for extending the system capacity to beyond 1 Tb/s. Channel multiplexing can be done in the time or the frequency domain through time-division multiplexing (TDM) and frequency-division multiplexing (FDM), respectively. To make the distinction explicit, it's common to refer to the two optical-domain techniques as optical TDM (OTDM) and wavelength-division multiplexing (WDM), respectively. The development of such multi-channel systems attracted considerable attention during the 1990s. [1.1]

The state of the art of fiber optic communication system has advanced dramatically during the relatively short period of past ten years. Generally, telecommunications networks are usually segmented in a three-tier hierarchy: access,

metropolitan, and long haul. Long haul/backbone networks span interregional/global distance and provide large tributary connectivity between regional and metro domains. By 2002, commercially available ultra long haul (>2000km) light-wave systems has exceeded 1.28Tb/s ($128 \times 10\text{Gbit/s}$), and the ultra high capacity light-wave systems (2.56Tb/s, $64 \times 40\text{Gbit/s}$), which capable of transmitting more than 1000km, are obtainable in the market as well. On the other end of the hierarchy are access networks, providing connectivity to a plethora of customers. Straddled in the middle are metropolitan (metro) networks, averaging regions between 10-100 km and interconnect access and long-haul networks. [1.2] [1.3]

1.2 Reconfigurable add/drop multiplexer

With the rapid progress of long haul transport systems in wide area networks (WANs), the bottleneck of light-wave system gradually shifts to metro area networks (MANs). To cater different service requirements and to cope with more diversified traffic patterns, metro networks need to provide more functionalities than long haul transport networks. Reconfigurable add/drop nodes will significantly enhance network flexibility and be able to provide the much needed functionalities.

Therefore, continuing improvement in optical component technologies and declining costs are making metro DWDM increasingly viable. These component technologies include lasers, amplifiers, filters, and switching devices. Multi-channel optical amplification was the primary enabler for long-haul DWDM, as increased amplifier spacing eliminated more costly electronic regenerators. As operators expand their networks and utilize more complex optical gear, optical amplifiers will be needed to compensate for transmission and nodal losses. Therefore, this is important topic to effectively decrease the number of the optical amplifiers in the metro networks.

Filtering is a key to wavelength channel management. Today, improving

technologies are yielding increasingly dense channel spacings and higher channel counts, for example, commercial 100GHz and 50GHz filters give 40 and 80 channels, respectively. Overall, three filter schemes are common in the metro, namely thin film, planar waveguides, and fiber-based grating. In them, planar waveguides, such as bulk arrayed waveguide gratings (AWG), can give 100-GHz spacing and lend well to high integration/channel counts, but its temperature stability and insertion losses need to be concern.

Optical loop experiments were performed as early as 1977 to study pulse propagation in multi-mode fiber. Circulating loop techniques, applied to an amplifier chain of modest length, are considered the most economic way of conducting transmission experiments. Without heavily invest in duplicated equipments, optical loop can provide an experimental platform to study a broad range of transmission phenomena with much longer transmission distance.

The system experiment will be constructed by re-circulating optical loop, the basic building block of an optical ring is the reconfigurable optical add/drop multiplexer (ROADM) node (Fig 1).

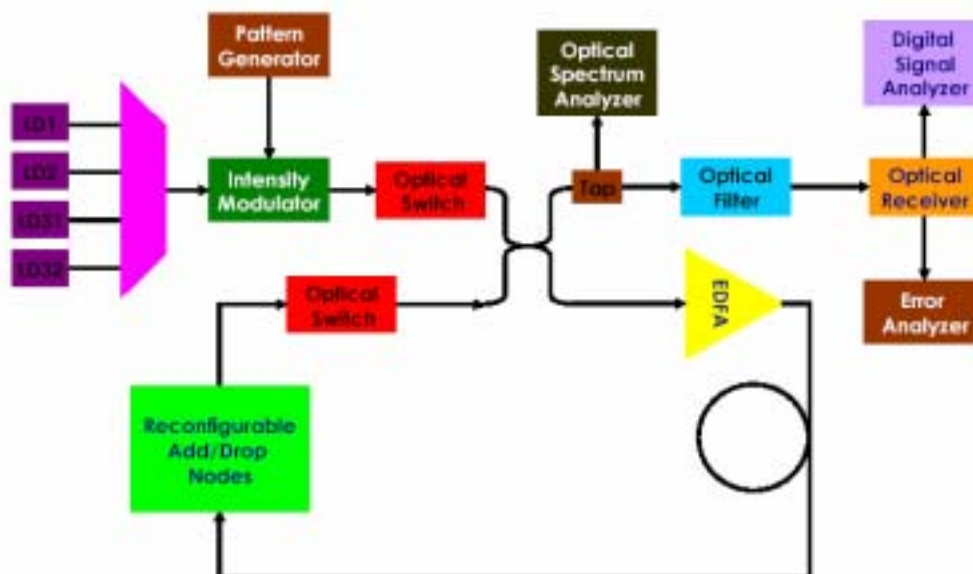


Fig. 1 The test platform of re-circulating optical loop for cascaded ROADMs.

1.3 Bi-directional transmission system

In future communication network, bidirectional transmission may be desirable for the capacity enhancement of existing systems and construction of reconfigurable and low-cost network. In economical aspect, bidirectional wavelength-division-multiplexing (WDM) transmission system are attractive, since they could reduce not only the use of fiber by a factor of two, but also the number of passive components, such as splitters in bidirectional multi-channel passive optical network. Transmitting bi-directionally over a single fiber can double the capacity of an installed unidirectional link. [1.5]

In bidirectional networks employing optical amplifiers, if signal are bi-directionally transmitted over a single fiber path, optical isolators cannot be used to prevent multiple reflections that can significantly degraded the receiver sensitivity. Therefore, system performances are severely degraded due to multiple reflections. It has been observed that due to multiple reflections along a fiber path, the laser phase noise is converted to the intensity noise, which may cause performance degradations in high speed lightwave system. Even if discrete reflections are carefully suppressed by using non-reflective connector facets, the multi Rayleigh backscattering (RB) in fibers give rise to the phase-to-intensity noise conversion. Furthermore, the interferometric noise from multiple RB increases proportionally with the optical amplifier gain. Thus, the maximum gain of inline optical amplifiers without optical isolator is limited to about 19 dB due to the additive intensity noise caused by RB.

The bidirectional add-drop multiplexer (ADM) is one of the key elements in bidirectional transmission WDM networks to increase the spectral efficiencies and reduce operation facilities of the unidirectional WDM system. The wavelength-interleaved bidirectional transmission reduces not only nonlinear effects

between adjacent channels, but also deployment and operation cost by sharing the same fiber for two opposite transmission directions in metro and access networks [3]. Recently, a bidirectional transmission was demonstrated by using a pair of WDM multiplexers, separated erbium-doped fiber amplifiers (EDFAs) and two optical circulators for each channel. We propose a novel structure for bidirectional transmission system which utilizes only one four-port interleaver and one dual-stage EDFA. The channel spacing of this interleaver is 50 GHz for multiplexing/de-multiplexing odd and even channels in a WDM system. This function of this four-port interleaver could lead bidirectional signals passing through the dual-stage EDFA in uni-direction so as to reduce the need of additional EDFA for bidirectional operation. Therefore, the RB could be decreased substantially. Finally, this configuration is applied to transmission system with metro add/drop applications. System experiment will be constructed as Fig.2 :

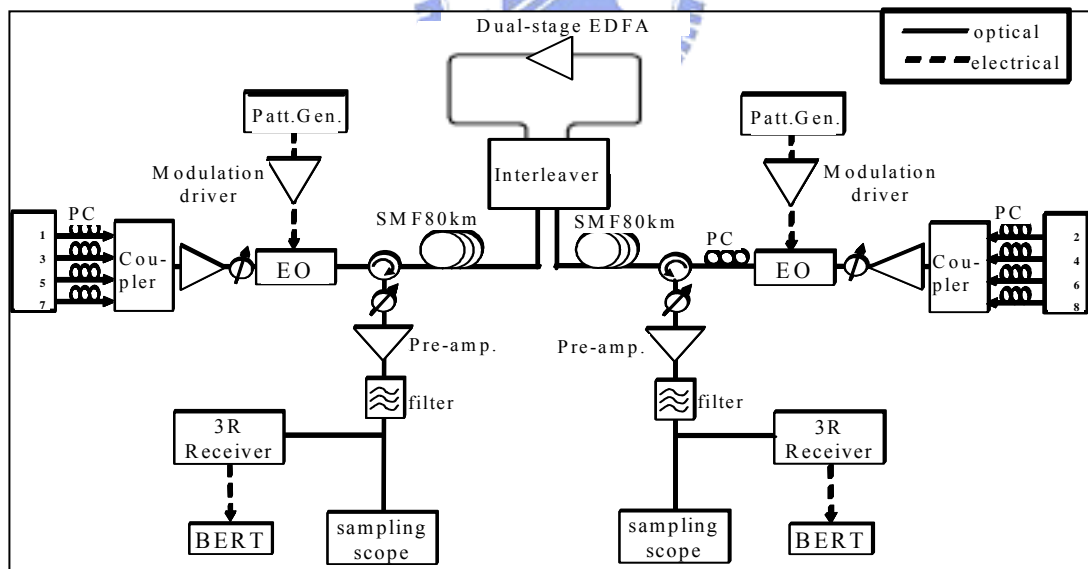


Fig.2 Experimental setup of a bi-directional transmission

References

- [1.1] “Fiber-optic communication systems”, Govind P.Agrawal, Wiley inter-science
- [1.2] P. V. Hatton, F. Cheston, “WDM Deployment in the Local Exchange Network,” *IEEE Communications Magazine*, Vol. 36, No. 2, February 1998, pp. 56-61
- [1.3] “Metro Optical Networks: Metro DWDM and the New Public Network,” *Pioneer Consulting Report*, 1999.
- [1.4] Jyehong Chen, 2003 NSC proposal.
- [1.5] “Estimation of performance Degradation of Bidirectional WDM transmission system due to Rayleigh Backscattering and ASE noise Using Numerical and analytical models”
- [1.6] J. L. Gimlett, M. Z. Iqbal, L. Curtis, N. K. Cheung, A. Righetti, F. Fontana, and G. Grasso, “Impact of multiple reflection noise in Gbit/s lightwave systems with optical fiber amplifiers,” *Electron. Lett.*, vol. 25, pp. 1393–1394, Sept. 1989.



Chapter 2

Interleaver

2.1 Introduction

An interleaver is a periodic optical filter that combines or separates a comb of dense wavelength-division multiplexed (DWDM) signals. The periodic nature of the interleaver filter reduces the number of Fourier components required for a flat passband and high-isolation rejection band. This is in contrast to single-channel add/drop filter that synthesize a single narrow-band filter over a wide rejection band. Because the interleaver requires fewer Fourier components, the same flat top, sharp edge response of a higher-order narrow-band filter can be realized with only a few sections.

The original design separates (or combines) even channels from odd channels across a DWDM comb. The filter function of an interleaver and its period are separable. The period is governed by the free-spectral range of the core elements, where narrower channel spacing is achieved by a longer optical path. Generally, the free-spectral range (FSR) of the interleaving filter is not accurately matched to the ITU grid and the center frequencies of the channels still may be offset error. Thermal dependence of the interleaver is the leading cause of offset error.

There are three broad classes of interleaver filter technologies: lattice filter (LF), Gires-Tournois based Michelson interferometer, and arrayed-waveguide router (AWG). Because the interleaver we used in the experiment is the lattice filter based interleaver, so this chapter will focus on the detail of the theory and design process of the LF interleavers. Also, the practical interleaver measurement will be shown to compare with the simulation results at the final section of this chapter.

2.2 Digital Concepts for Optical Filters

Digital filter, or discrete time filter, has been widely used in digital electronic circuit. The advantages of relating digital and optical filters are that numerous algorithms developed for digital filters can be used to design optical filters. Borrowed from the electronic world, optical engineer follows the same concept and uses optical delay line to create the desired filter function. Depending on whether the transfer function has poles, an optical filter can be classified as a finite impulse response filter and an infinite impulse response filter. Before describing the design process of the interleaver filter, the basic knowledge about the representations of digital signals, the Z-transform, the zeros, and the poles were needed to be introduced in followed sub-sections.

2.2.1 Discrete Signals and Z-transform

A similar set of properties applied for discrete signals. A discrete signal can be obtained by sampling a continuous time signal $x(t)$ at $t = nT$ where the sampling interval is, T and n is the sample number. For a digital filter, T is the unit delay associated with the discrete impulse response. The impulse response of an optical filter, where each stage has a delay that is an integer multiple of the unit delay, is described by a discrete sequence. The Fourier transform of a sequence has a sum instead of an integral as follows:

$$X(f) = \sum_{n=-\infty}^{\infty} x(nT) e^{-j2\pi fnT} \quad (1)$$

where f denote the absolute frequency. A normalized frequency is defined as $\nu \equiv fT = f / FSR$, where the free spectral range (FSR) is the period of the absolute frequency response. The normalized angular frequency is given by $\omega = 2\pi\nu$. A discrete signal is often represented by $x(n)$, leaving T implied. The discrete-time Fourier transform (DTFT) is defined as

$$X(\nu) = \sum_{n=-\infty}^{\infty} x(n)e^{-j2\pi\nu n} \quad (2)$$

The Z-transform is an analytic extension of the DTFT for discrete signals, similar to the relationship between the Laplace transform and the Fourier transform for continuous signals. The Z-transform is defined for a discrete signal by substituting z for $e^{j\omega}$ in Eq. (2) as follows:

$$H(z) = \sum_{n=-\infty}^{\infty} h(n)z^{-n} \quad (3)$$

where $h(n)$ is the impulse response of a filter or the values of a discrete signal, and z is a complex number that may have any magnitude. For the power series to be meaningful, a region of convergence must be specified, for example $r_{\min} \leq |z| \leq r_{\max}$

where r_{\min} and r_{\max} are radii. Of particular interest is $|z|=1$, called the unit circle, because the filter's frequency response is found by evaluating $H(z)$ along $z = e^{j\omega}$. The inverse Z-transform is found by applying the Cauchy integral theorem to Eq. (3) to obtain:

$$h(n) = \frac{1}{2\pi j} \oint H(z)z^{n-1} dz \quad (4)$$

The convolution resulting from filtering in the time domain

$$y(n) = x(n) * h(n) = \sum_{m=-\infty}^{\infty} x(m)h(n-m) \quad (5)$$

reduces to multiplication in the Z-domain.

$$Y(z) = H(z)X(z) \quad (6)$$

Equation (6) shows that a filter's transfer function, $H(z)$, can be obtain by dividing the output by the input in the Z-domain.

$$H(z) = \frac{Y(z)}{X(z)} \quad (7)$$

A fundamental property of the Z-transform relates $h(n-1)$ to $H(z)$ as shown in Eq. (8)

$$\sum_{n=-\infty}^{\infty} h(n-1)z^{-n} = z^{-1} \sum_{n=-\infty}^{\infty} h(n)z^{-n} = z^{-1}H(z) \quad (8)$$

The impulse response is assumed to be causal so that $h(n) = 0$ for $n < 0$. One delay results in multiplication by z^{-1} in the Z-domain, and a delay of N units results in multiplication by z^{-N} .

The Z-transforms are introduced for two examples here. First, let the output of a filter be the sum of the last $N + 1$ inputs: $y(n) = x(n) + x(n-1) + \dots + x(n-N)$. Such a filter contains N delays, which are feed-forward paths. The impulse response is $h(n) = \delta(n) + \delta(n-1) + \dots + \delta(n-N)$.

The transfer function is $H(z) = 1 + z^{-1} + \dots + z^{-N} = (1 - z^{-(N+1)}) / (1 - z^{-1})$.

There are N roots of $H(z)$ which all occur on the unit circle. For second example, let the output of a filter be given as $y(n) = ay(n-1) + x(n)$, where a is a real number satisfying $0 \leq |a| < 1$ and $n \geq 0$. This filter contains one delay, which is a feedback path. Its Z-transform is $Y(z) = az^{-1}Y(z) + X(z)$, which gives the transfer function $H(z) = Y(z) / X(z) = 1 / (1 - az^{-1})$. The transfer function is equivalent to the infinite sum

$$H(z) = \sum_{n=-\infty}^{\infty} a^n z^{-n} = \frac{1}{1 - az^{-1}} \quad (9)$$

The region of convergence is $|z| > a$.

2.2.2 Poles and Zeros

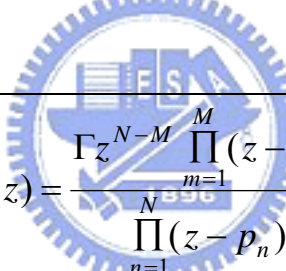
A discrete linear system with a discrete input signal in Eq. (10) as follows:

$$y(n) = b_0x(n) + b_1x(n-1) + \dots + b_Mx(n-M) - a_1y(n-1) - \dots - a_Ny(n-N) \quad (10)$$

The weights are given by the a and b coefficients. The Z-transform results in a transfer function that is a ratio of polynomials.

$$H(z) = \frac{\sum_{m=0}^M b_m z^{-m}}{1 + \sum_{n=1}^N a_n z^{-n}} = \frac{B(z)}{A(z)} \quad (11)$$

$A(z)$ and $B(z)$ are M th and N th-order polynomials, respectively. The expression for $H(z)$ can also be written in terms of the roots of the polynomials as follows [2.5]:



$$H(z) = \frac{\Gamma z^{N-M} \prod_{m=1}^M (z - z_m)}{\prod_{n=1}^N (z - p_n)} \quad (12)$$

The zeros of the numerator are represented by z_m . A zero that occurs on the unit circle, $|z_m| = 1$, results in zero transmission at that frequency. The roots of the denominator polynomial are designed by p_n . The Γ has a maximum value determined by $\max\{|H(z)|_{z=e^{j\omega}}\} = 1$.

Digital filters are classified by the polynomials defined in Eq. (11). A moving average (MA) filter has only zeros and also belongs to a finite impulse response. It consists only of feed-forward paths. A single stage MA digital filter is shown in Figure 2.1(a). An autoregressive (AR) filter has only poles and contains one or more feedback paths as shown in Fig. 2.1(b). A pole produces an impulse response with

an infinite number of terms in contrast to the finite number of terms for MA filters.

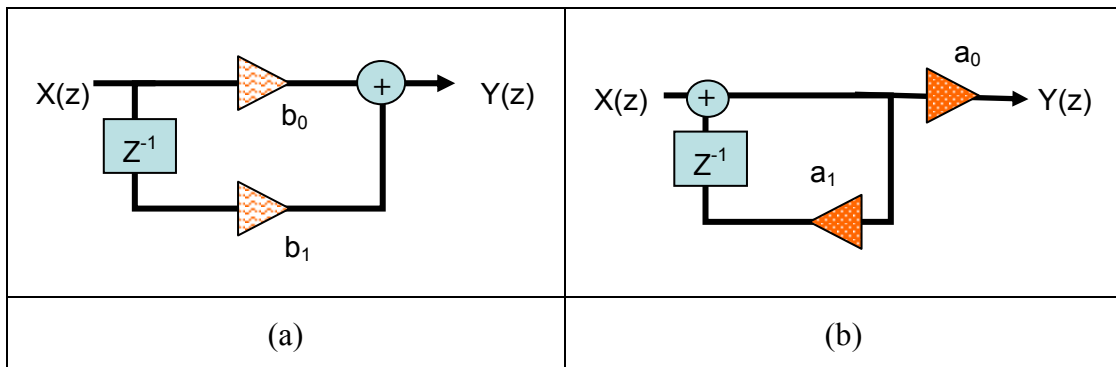
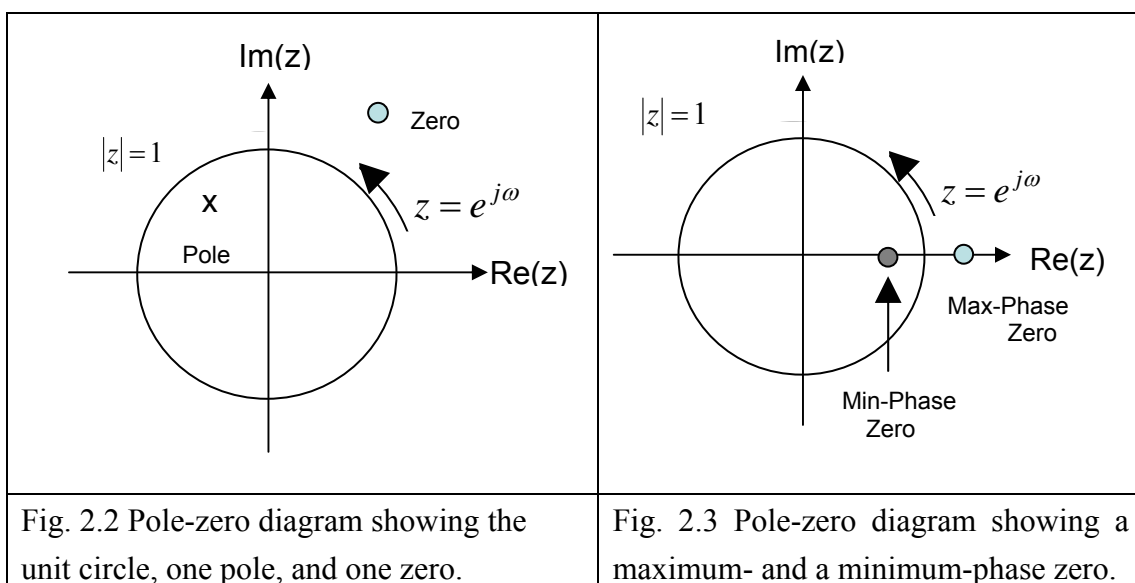


Fig. 2.1 Illustrations of single-stage (a) MA digital filter and (b) AR digital filter.

2.2.3 Magnitude Response and Group Delay

A filter's magnitude response is equal to the modulus of its transfer function, $|H(z)|$, evaluated at $z = e^{j\omega}$. Based on the pole/zero representation of $H(z)$, only the distance of each pole and zero from the unit circle affects the magnitude response, i.e. $|e^{j\omega} - z_m|$ or $|e^{j\omega} - p_n|$. One trip around the unit circle is equal to one FSR. A convenient graphical method for estimating a filter's response is shown in figure 2.2. Zeros with a magnitude >1 are called maximum-phase, and those with magnitudes <1 are called minimum-phase. A pole-zero diagram with a pair of zeros that are located reciprocally about the unit circle is shown in Fig. 2.3.



The filter's group delay is defined as the negative derivative of the phase of the transfer function with respect to the angular frequency as follows:

$$\tau_g = T \times \tau_n = T \times \left[-\frac{d}{d\omega} \tan^{-1} \left(\frac{\text{Im}\{H(z)\}}{\text{Re}\{H(z)\}} \right) \right]_{z=e^{j\omega}} \quad (13)$$

where τ_n is normalized to the unit delay, T . The absolute group delay is given by $\tau_g = T \times \tau_n$. To obtain the group delay for a single zero, considering the transfer function $H_{1-zero}(z) = 1 - re^{j\phi}z^{-1}$ where r and ϕ are the magnitude and phase of the zero. By substituting $z = e^{j\omega}$ in $H_{1-zero}(z)$, the phase is derived in terms of r , ϕ , and ω as follows:

$$\Phi_{1-zero} = \tan^{-1} \left[\frac{r \sin(\omega - \phi)}{1 - r \cos(\omega - \phi)} \right] \quad (14)$$

$$\frac{d \tan^{-1}[g(x)]}{dx} = \frac{g'(x)}{1 + g^2(x)} \quad (15)$$

where Φ_{1-zero} is the phase of $H_{1-zero}(z)$. Borrowed from Eq. (15), the group delay simplifies to

$$\tau_{1-zero}(r, \phi) = \frac{r[r - \cos(\omega - \phi)]}{1 - 2r \cos(\omega - \phi) + r^2} \quad (16)$$

Then, consider the transfer function, $H_{1-zero}(z) = re^{-j\phi} - z^{-1}$, with the reversed path, the group delay is

$$\tau_{1-zero}\left(\frac{1}{r}, \phi\right) = \frac{[1 - r \cos(\omega - \phi)]}{1 - 2r \cos(\omega - \phi) + r^2} = 1 - \tau_{1-zero}(r, \phi) \quad (17)$$

The sum of the group delays is a constant value indicating that the filter has linear phase with the same magnitude response as shown in Fig. 2.4.

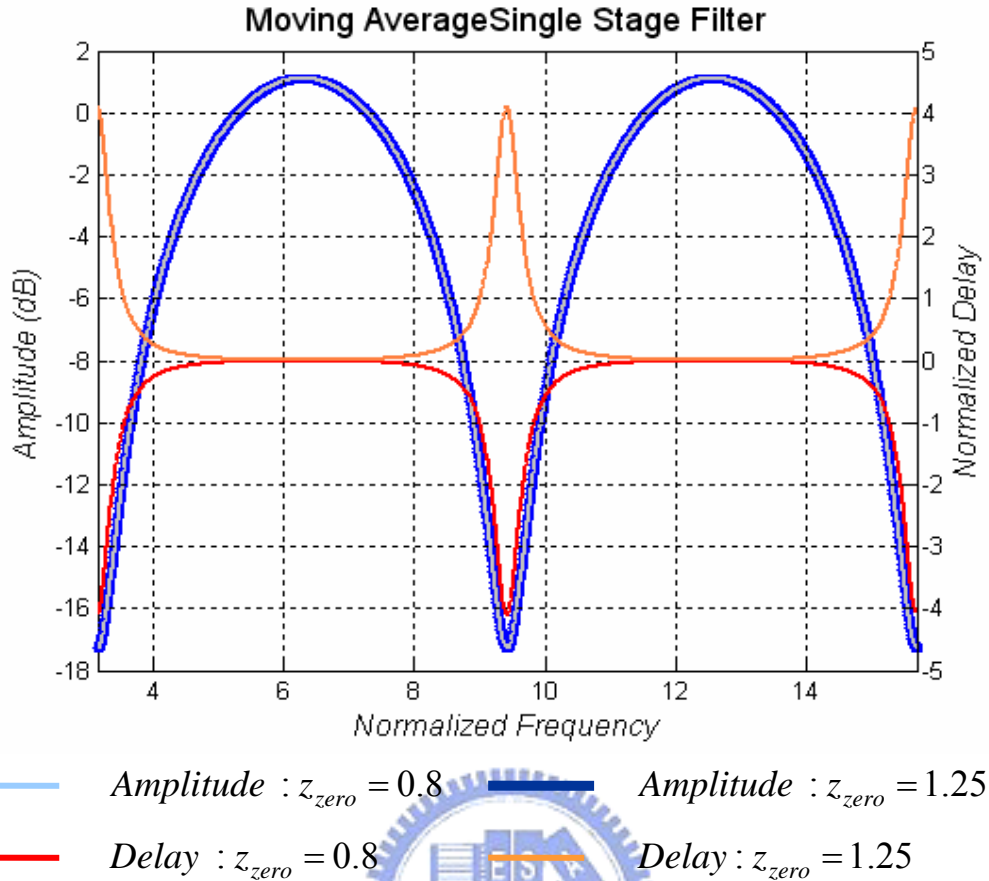


Fig. 2.4 Phase response of maximum and minimum phase MA filters.

2.3 Interleaver

2.3.1 Interleaver technology approaches

There are three broad classes of interleaver filter technologies: lattice filter (LF), Gires-Tournois based Michelson interferometer, and arrayed-waveguide router (AWG). Within the lattice filter class there is the birefringent filter, employing birefringent crystals and classically known as a Lyot or Solc filter; the glass-based filter which substitutes an artificial polarization-dependent delay for the birefringent elements of the preceding type; and the Mach-Zehnder filter, which is the analog to the Lyot filter and is generally made with planar waveguides. Within the Gires-Tournois (GT) class there is the interference filter and the birefringent analog (B-GT) [refs]. Arrayed-waveguide routers have designs for single-channel and banded filters.

2.3.2 Lattice Interleaver

Lattice filters are made from a cascade of differential-delay elements where the differential-delay of each element is an integral multiple of a unit delay and power is exchanged across paths between the elements. There are three issues to address in the study of lattice filters: the realization of the unit cell that generates the differential delay; the number of unit cells and associated intermediate power exchange; and the cascade of multiple filters.

Figure 2.5 shows the configuration of the interleaver consisted of the birefringent crystals. The basic principle is based on interference between polarized light, which depends on phase retardation between the components of light polarized parallel to the slow and the fast axes of the crystal. Consequently, birefringent crystal is used to perform as optical delay, and a half-wave plate is used to change the polarization direction between the delay components. An optical FIR digital filter can, thus, be made by cascading delay lines and controlling the angle of rotation between half-wave plates. The half-wave plates can also be considered to be rotated to generate required Fourier frequency components.

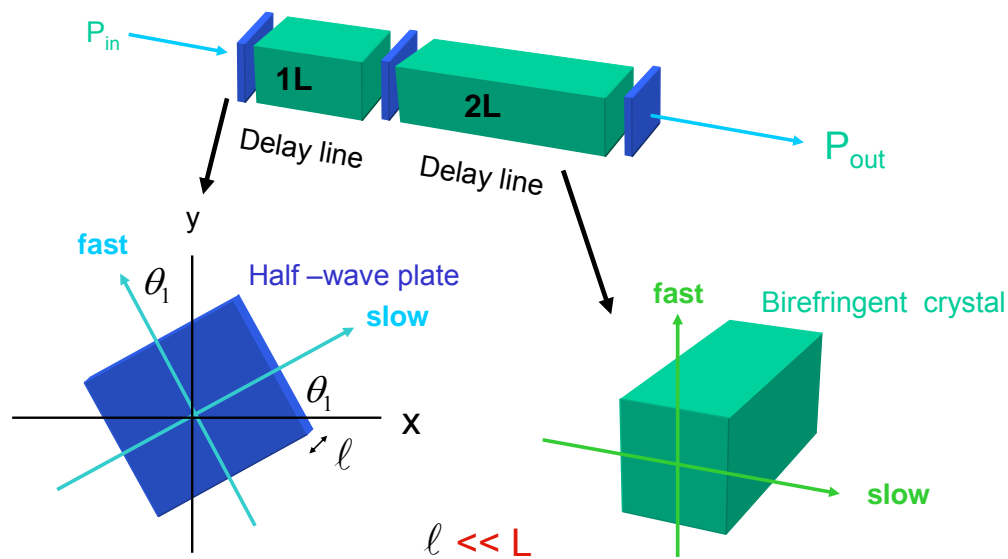


Fig. 2.5 Brief configuration of an L-2L interleaver

Actually, the goal of design is to generate a periodic rectangular function as shown in Fig. 2.6.

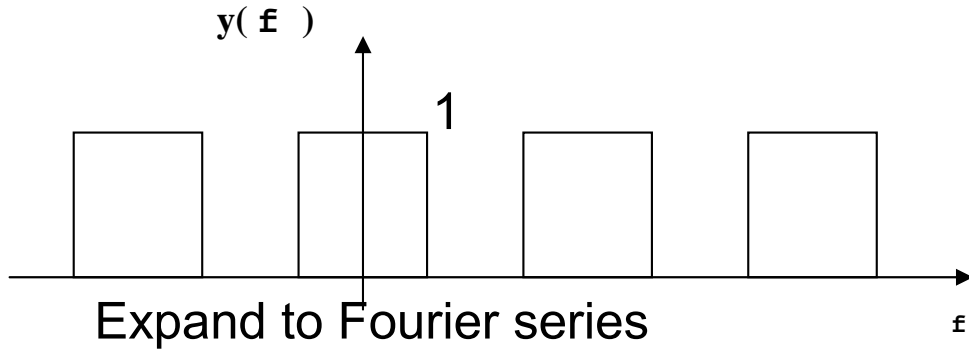


Fig. 2.6 The Fourier series function with periodic.

The function could be defined to

$$y(f) = \begin{cases} 0 & , -50 < f < -25 \\ 1 & , -25 < f < 25 \\ 0 & , 25 < f < 50 \end{cases} , y(f) = y(f + 100) \quad (21)$$

Expand it to a Fourier series, there is no even function term in it. The constant a_0 and a_n is retained.

$$a_0 = \frac{1}{200} \int_{-50}^{50} 1 \cdot df = \frac{1}{2} \quad (22)$$

$$a_n = \frac{1}{100} \int_{-50}^{50} 1 \cdot \cos(n2\pi f) \cdot df = \frac{2}{n\pi} \sin\left(\frac{n\pi}{2}\right) , n = 1, 2, 3 \dots$$

Then the final rectangular function will be written to the Eq. (23)

$$y(f) = \frac{1}{2} + a_1 \cdot \cos(2\pi f) - a_3 \cdot \cos(3 \times 2\pi f) + \dots \quad (23)$$

Here we know that the square-wave amplitude function has only odd Fourier frequency components with appropriate Fourier coefficients.

According to the Jones matrix theory, a half-wave plate has a phase retardation of $\Gamma = \pi$, and the thickness of $\ell = \lambda/2(n_e - n_o)$. The Jones matrix for the half-wave plate is obtained by using Eq. 24.

$$W_{hp} = \begin{bmatrix} 0 & -i \\ -i & 0 \end{bmatrix} \quad (24)$$

We can write the Jones matrix for the delay line as

$$W_{delay} = \begin{bmatrix} e^{-i\frac{\omega}{2}dnL} & 0 \\ 0 & e^{i\frac{\omega}{2}dnL} \end{bmatrix} \quad (25)$$

where L is the length of the delay-line crystal and dn is the difference between the n_e and n_o (the indices are the ordinary and extraordinary axes).

Considering the incident light beam with polarization state described by the Jones vector $v = \begin{pmatrix} v_x \\ v_y \end{pmatrix}$, where v_x and v_y are two complex numbers. The x and y axes

are fixed laboratory axes. To determine how the light propagates in the retardation plate, we need to decompose the light into a linear combination of the “fast” and “slow” eigenwaves of the crystal. This is done by the coordinate transformation:

$$\begin{pmatrix} v_s \\ v_f \end{pmatrix} = \begin{pmatrix} \cos\psi & \sin\psi \\ -\sin\psi & \cos\psi \end{pmatrix} \begin{pmatrix} v_x \\ v_y \end{pmatrix} \equiv R(\psi) \begin{pmatrix} v_x \\ v_y \end{pmatrix}.$$

v_s is the slow component of polarization vector V , whereas v_f is the fast component.

The “slow” and “fast” axes are fixed in the crystal. These two components are eigenwaves of the retardation plate and will propagate with their own phase velocities and polarization. The Jones vector of the polarization state of the emerging beam in the xy coordinate is given by transforming back from the crystal sf coordinate system:

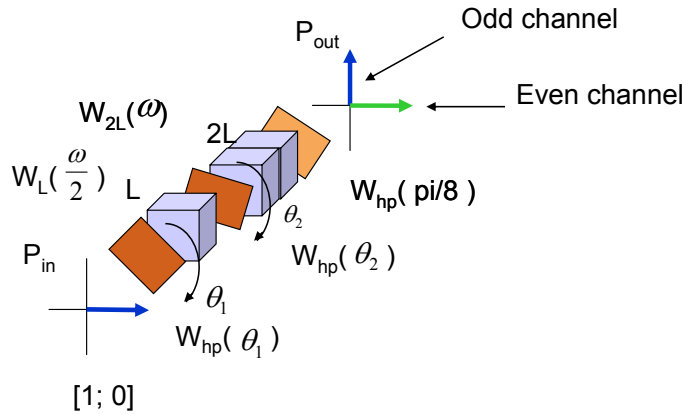
$$\begin{pmatrix} v_x' \\ v_y' \end{pmatrix} = \begin{pmatrix} \cos\psi & -\sin\psi \\ \sin\psi & \cos\psi \end{pmatrix} \begin{pmatrix} v_s' \\ v_f' \end{pmatrix} \equiv R(-\psi) \begin{pmatrix} v_s' \\ v_f' \end{pmatrix}. \quad \text{So we can write the}$$

transformation due to the retardation plate: $\begin{pmatrix} v_x' \\ v_y' \end{pmatrix} = R(-\psi)W_0R(\psi) \begin{pmatrix} v_x \\ v_y \end{pmatrix} = W(\psi) \begin{pmatrix} v_x \\ v_y \end{pmatrix}$

Change the angle of the two half-wave plates to fit the Fourier series

For Example: 1L-2L

$$\begin{bmatrix} e^{-i\frac{\omega}{2}dnL} & 0 \\ 0 & e^{i\frac{\omega}{2}dnL} \end{bmatrix}$$



$$P_{out} = W_{hp}(22.5^\circ) * W_{2L}(\omega) * W_{hp}(\theta_2) * W_L(\omega/2) * W_{hp}(\theta_1) * P_{in}$$

In Fig above, the Jones matrix for the incident beam can be written as $[1;0]$ to specify the input light being linearly polarized on the x axis. By adjusting the angles of the half-wave plates appropriately and let the last , we can get the odd channels and even channels lying the x and y axes , respectively, at the output port.

By combining all Jones matrices of the birefringent crystals, we can write the transmission as

$$T = W_{hp}(22.5^\circ) * W_{delay}(2L) * W_{hp}(\theta_2) * W_{delay}(L) * W_{hp}(\theta_1) \quad (26)$$

$$E_{out} = T * E_{in}$$

where $W_{delay}(2L)$ and $W_L(L)$ are the Jones matrices of the two crystals

But the problem is how to get the angles to fit the Fourier coefficients in Eq. (22)?

The answer is that we can use the optimization tools in Matlab programs. The goal is minimizing the error function by sweeping the half-wave plate angles as

$$\begin{aligned}
error &= \max |y(w) - x(w)| \\
error &= \int_{w_1}^{w_2} |y(w) - x(w)| dw \\
error &= \int_{w_1}^{w_2} |y(w) - x(w)|^2 dw \quad w_1 = w_c - \frac{FSR}{2}, w_2 = w_c + \frac{FSR}{2} \quad (27) \\
error &= \int_{w_1}^{w_2} \left| \log_{10}^{y(w)^2} - x(w) \right|^2 dw
\end{aligned}$$

where $x(w)$ is the target or ideal square periodic function and the $f(w)$ is real transmission function. The transmission function is periodic, so the errors are only summed over one FSR at the central frequency w_c . The last three approximation criteria include errors at all points of frequency in the interval; therefore, they include more error data than the first for each $y(w)$ considered. We choose the last approximation criterion because it is the energy in the error signal.

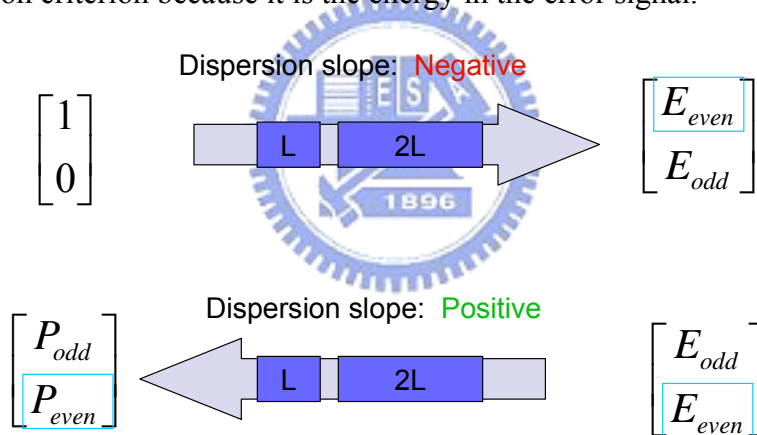


Fig. 2.7 Dispersion free path

Figure 2.7 shows the opposite slopes of the dispersion from the opposite paths. It is the key point is to exchange the positions of E_{even} and E_{odd} , and get them into the opposite direction.

2.3.3 Mathematical Derivation

Here we use the easiest case: one stage interleaver includes a delay line and two half-wave plates in which the second plate is determined to 22.5 degree. Assume

that there is an incident beam $V_x (= \begin{bmatrix} 1 \\ 0 \end{bmatrix})$ injected to the first half-wave plate, then the

Jones matrix M_1 at the output can be written as

$$\begin{aligned}
 M_1 &= \begin{bmatrix} \cos \theta_1 & -\sin \theta_1 \\ \sin \theta_1 & \cos \theta_1 \end{bmatrix} \cdot \begin{bmatrix} e^{-j\frac{\pi}{2}} & 0 \\ 0 & e^{j\frac{\pi}{2}} \end{bmatrix} \cdot \begin{bmatrix} \cos \theta_1 & \sin \theta_1 \\ -\sin \theta_1 & \cos \theta_1 \end{bmatrix} \cdot \begin{bmatrix} 1 \\ 0 \end{bmatrix} \\
 &= \begin{bmatrix} e^{-j\frac{\pi}{2}} \cos^2 \theta_1 + e^{j\frac{\pi}{2}} \sin^2 \theta_1 \\ e^{-j\frac{\pi}{2}} \cos \theta_1 \sin \theta_1 - e^{j\frac{\pi}{2}} \cos \theta_1 \sin \theta_1 \end{bmatrix} = j \cdot \begin{bmatrix} a_1(\theta_1) \\ a_2(\theta_2) \end{bmatrix} \quad (28) \\
 &\dots\dots(a_1 \text{ and } a_2 \text{ are real numbers})
 \end{aligned}$$

where the undetermined angle is set to be a variable θ_1 . Regard M_1 as the emerging beam and let it inject into the crystal of length L. The new Jones matrix M_2 is obtained by using Eq. (29).

$$M_2 = e^{-j\phi} \cdot \begin{bmatrix} e^{-j\frac{\pi f}{df_c}} & 0 \\ 0 & e^{j\frac{\pi f}{df_c}} \end{bmatrix} \cdot j \cdot \begin{bmatrix} a_1 \\ a_2 \end{bmatrix} = j \cdot \begin{bmatrix} a_1 e^{-j\frac{\pi f}{df_c}} \\ a_2 e^{j\frac{\pi f}{df_c}} \end{bmatrix} \quad (29)$$

In Eq. (29), df_c is the channel spacing and ϕ is equal to $dn\omega L/2c$. The phase factor $e^{-j\phi}$ can be neglected if interference effects are not important, or not observable. Then use M_2 to multiply the second half-wave plate

$(W_{22.5^\circ} = j \begin{bmatrix} X & Y \\ Y & -X \end{bmatrix}, X \text{ and } Y \text{ are real numbers})$ with the angle of 22.5 degree as shown in Eq. (30).

$$\begin{aligned}
M_3 &= W_{22.5^\circ} \cdot M_2 = j \begin{bmatrix} X & Y \\ Y & -X \end{bmatrix} \cdot j \begin{bmatrix} a_1 e^{-j\frac{\pi f}{df_c}} \\ a_2 e^{j\frac{\pi f}{df_c}} \end{bmatrix} \\
&= - \begin{bmatrix} a_1 X e^{-j\frac{\pi f}{df_c}} + a_2 Y e^{j\frac{\pi f}{df_c}} \\ a_1 X e^{-j\frac{\pi f}{df_c}} - a_2 Y e^{j\frac{\pi f}{df_c}} \end{bmatrix} = \begin{bmatrix} E_x \\ E_y \end{bmatrix}
\end{aligned} \tag{30}$$

In Eq. (30), we arbitrarily choose E_x or E_y and square it to obtain the Eq. (31).

$$\begin{aligned}
T_x &= E_x \cdot E_x^* = (a_1 X + a_2 Y)^2 \cos^2 \frac{\pi f}{df_c} + (a_1 X - a_2 Y)^2 \sin^2 \frac{\pi f}{df_c} \\
&= [a_1(\theta_1)X]^2 + \left\{ [a_2(\theta_2)Y]^2 + 2a_1(\theta_1)Xa_2(\theta_1)Y \right\} \cos \frac{2\pi f}{df_c}
\end{aligned} \tag{31}$$

Compare with Eq. (23), the first term needs to equal 1/2 and the coefficient of the second term needs to equal the Fourier coefficient by optimizing the angle of θ_1 .

By this way, we can easy to understand the theory of interleaver.

2.3.4 Interleaver Simulation Results & Practical Device Measurement

The lengths of delay-line crystals in the program are determined using Eq. (32).

$$\begin{aligned}
f_c &= m \frac{c}{dnL} \Rightarrow L = \frac{f_c dn}{mc} \\
df_c &= \text{Channel spacing} = \text{FSR}
\end{aligned} \tag{32}$$

In Eq. (32), c is the speed of light; f_c is the central frequency in the range of operation frequencies; m is the order of the birefringent wave plate.

1. L-2L Interleaver

The found angles for two half-wave plates are 7.7356 and 29.5286 degrees. Figure 2.8 shows the transmission responses of the even and odd channels; the isolation is about 17 dB.

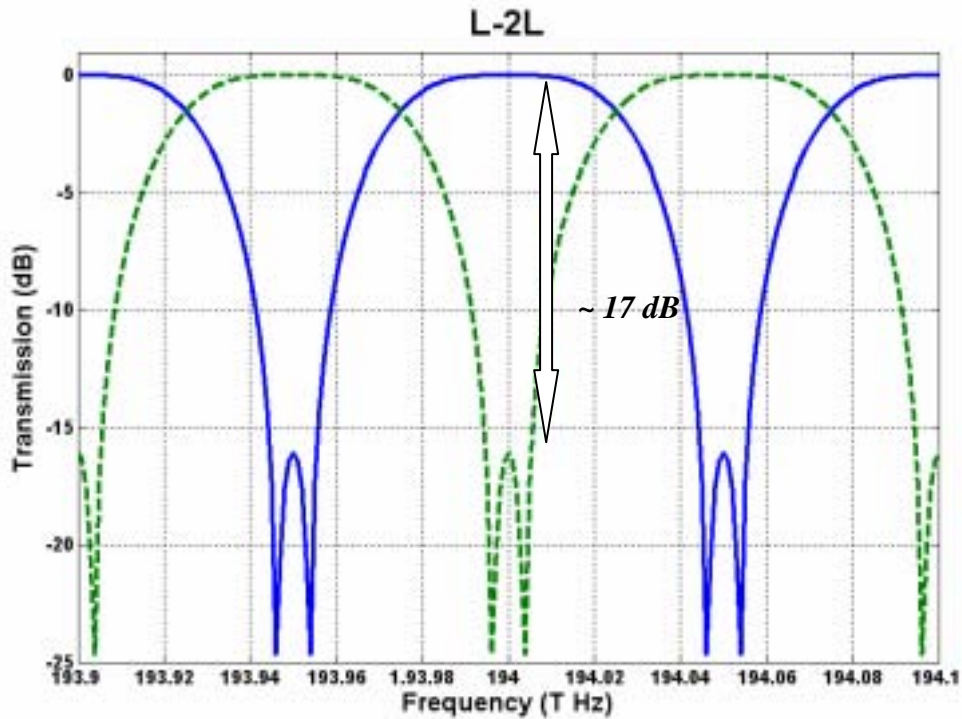


Fig. 2.8 Transmission responses of the even and odd channels.

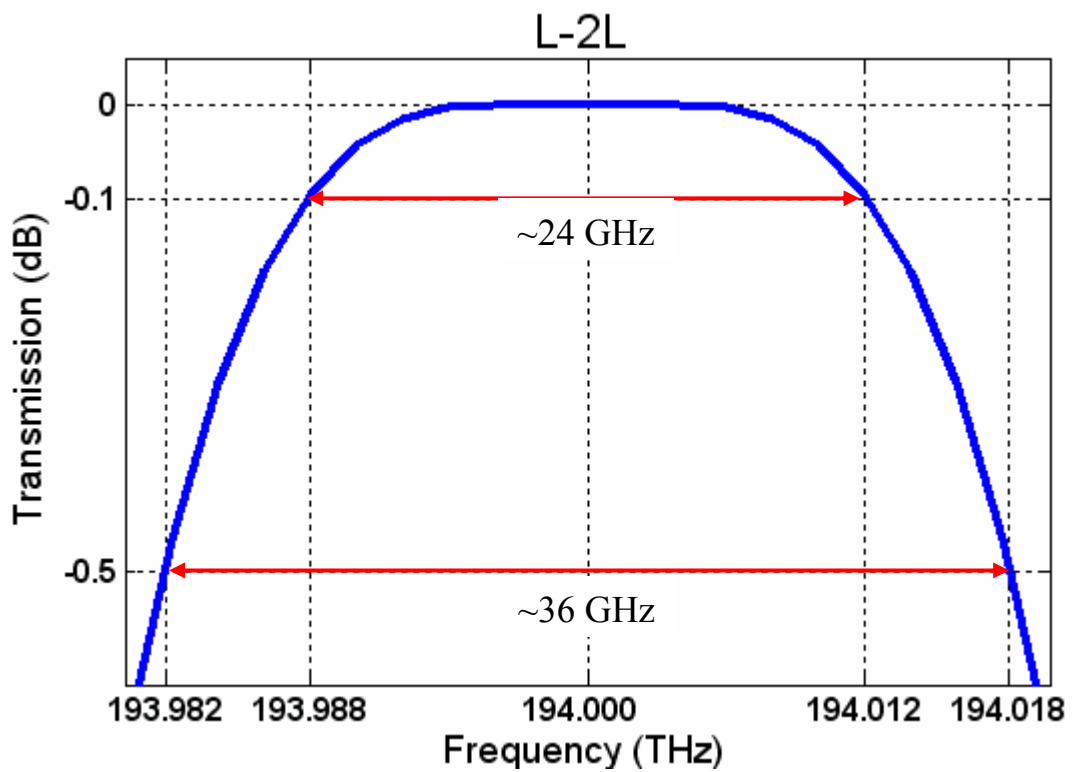


Fig. 2.9 The bandwidth estimations of -0.1dB and -0.5dB for L-2L interleaver.

The ripple is about 0.0026 dB; the bandwidths of -0.1dB and -0.5dB are 24 GHz (channel spacing) and 36 GHz, respectively, as shown in Fig. 2.9.

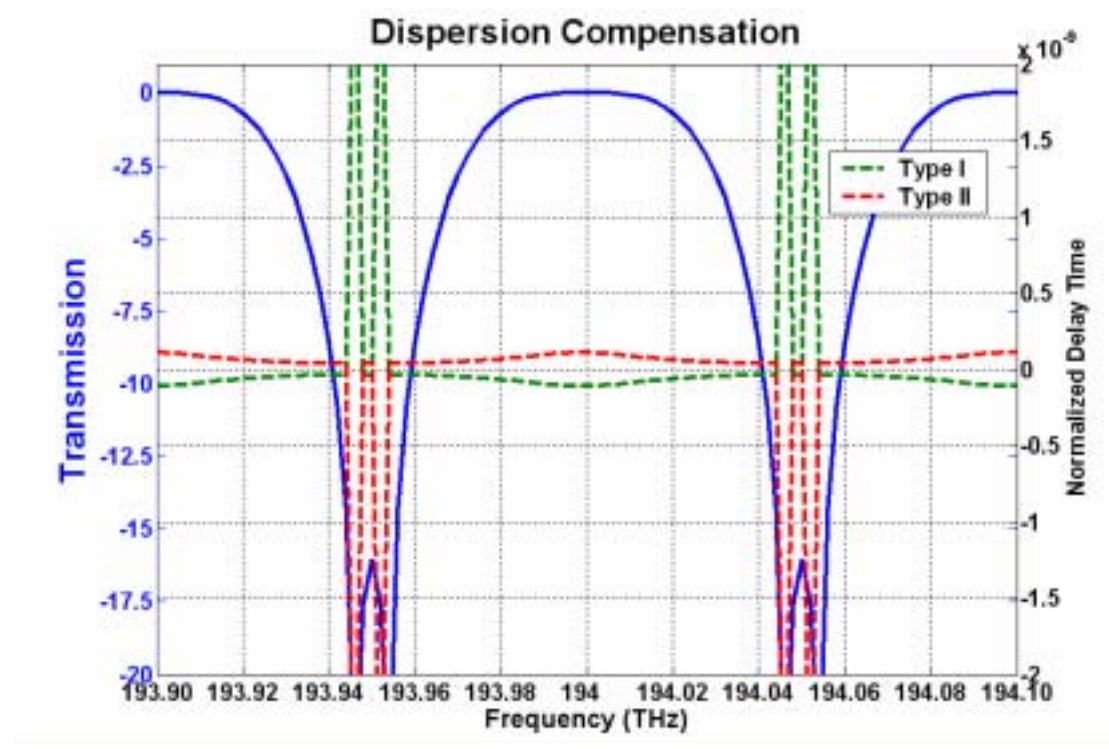


Fig. 2.10 Dispersion compensating interleavers for add/drop node

In Fig. 2.10, the path with the negative group delay is called type-A here, and another path with the positive group delay is called type-B. The type-A and type-B have the same transmission response.

The corresponding parameters for simulation are given below:

Central wavelength = 194.00 THz;

Difference of index between n_0 and $n_e=0.2138$;

$c=2.997925 \times 10^8$ m/s;

ch=50 GHz;

The interleaver we used is a symmetrical four-port interleaver with two input and two output ports. The detail configuration is shown in Fig. 2.11. It incorporates the birefringent crystal cells; half wave plates (HWP), YVO4 walk off crystals (YWC) and polarization beam splitters (PBS).

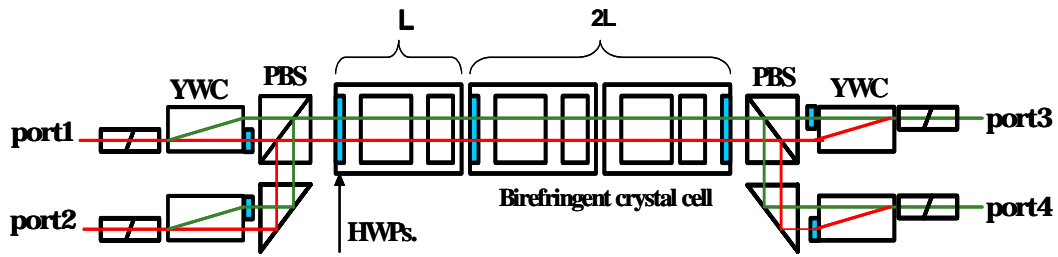


Fig. 2.11 Detail configuration of an L-2L interleaver

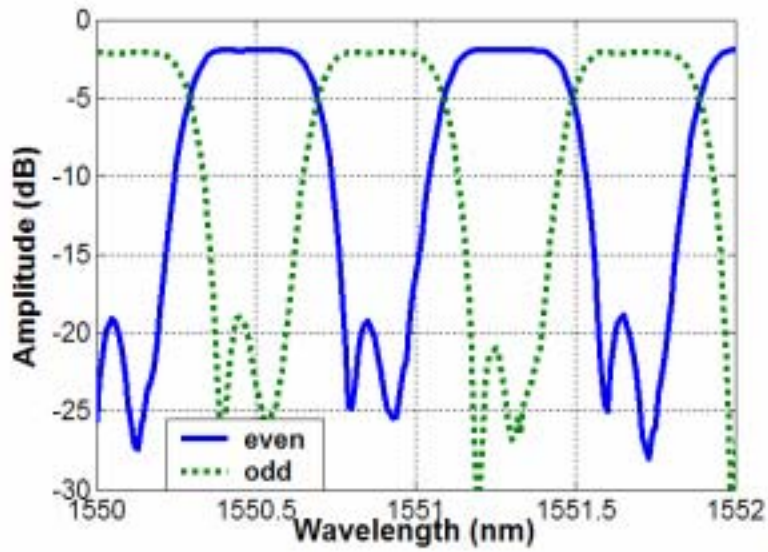


Fig. 2.12. Measured amplitude response of the interleaver for even and odd channels

Figure 2.12 illustrates the measured amplitude response of the interleaver for even and odd channels. The channel spacing of this interleaver is 50-GHz with insertion loss of 2.2-dB and 0.5-dB pass band of around 35-GHz, respectively. The two mirrored corresponding group delay curves are measure by the channel analyzer (Q7760), showed in figure 2.13(a) and figure 2.13(b).

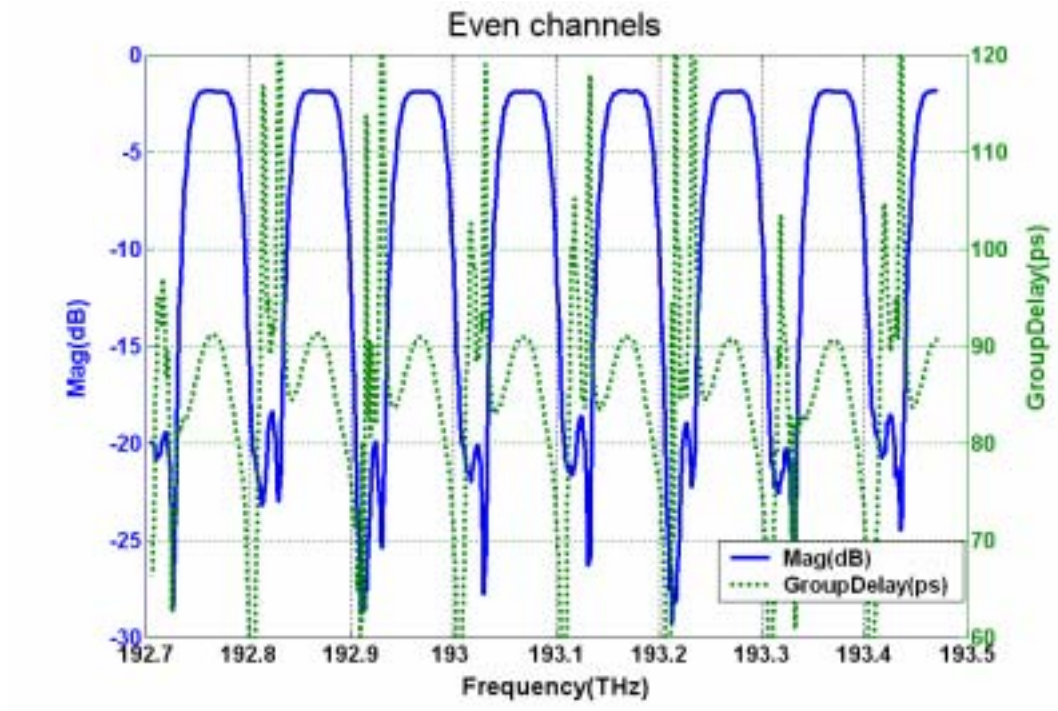


Fig. 2.13(a). Amplitude response and the corresponding group delay of the interleaver for even channels (type I)

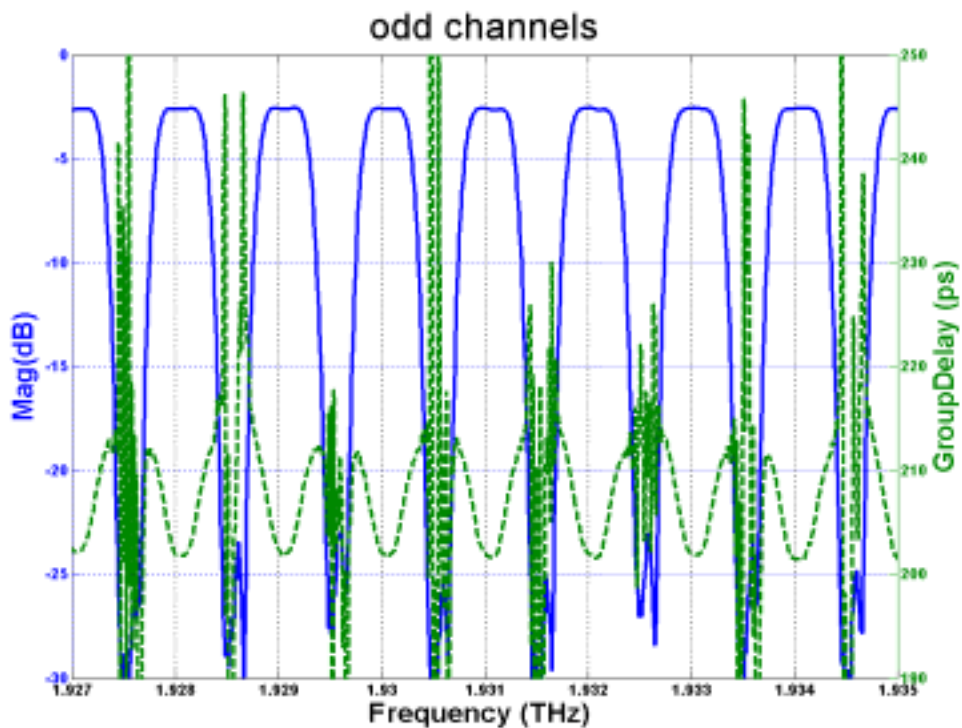


Fig. 2.13(a). Amplitude response and the corresponding group delay of the interleaver for even channels (type II)

References

- [2.1] S. Cao, J. Chen, J. N. Damask, C. R. Doerr, L. Guiziou, G. Harvey, Y. Hibino, S. Suzuki, K.-Y. Wu, P. Xie, “*Interleaver Technology: Comparisons and Applications Requirments*,” OFC’03.
- [2.2] Benjamin B. Dingel, “*Properies of a Novel Noncascaded Type, Easy-to-Design, Ripple-Free Optical Bandpass Filter*,” Journal of Lightwave technology, vol. 19, No. 8. August 1999.
- [2.3] A. V. Oppenheim, et al., “*Discrete-Time Signal Processing*,” 2nd ed., Prentice Hall, New Jersey
- [2.4] Christi. K. Madsen, Jian H. Zhao, et al., “*Optical Filter Design and Analysis: A Signal Processing Approach*,” Wiley Interscience.
- [2.5] A. Oppenheim and R. Schafer, Digital Signal Processing, 2nd. Ed., Englewood, N.J.: Prentice-Hall, Inc., 1975.
- [2.6] Hermann A. Haus, et al., “*Waves and Fields in Optoelectronics*,” Prentice-Hall.
- [2.7] A. Yariv, P. Yeh, “*Optical Waves in Crystals*,” Mei Ya.
- [2.8] J. Chen, “Dispersion Compensated Interleaver Pairs for 40 Gb/s Metro Add/Drop Applications”.
- [2.9] Gordon E. Carlson, “*Signal and Linear System Analysis*,” wiley.

Chapter 3

Re-circulating loop experiment for testing the cascadability of interleaver pair

3.1 Type AA and Type AB connection for an interleaver pair

Many DWDM systems have used interleavers as multiplexers and de-multiplexers. In a metro system, a pair of interleavers can be used in add/drop applications to provide up to 50% adding and dropping of total traffic while simultaneously reducing the insertion loss associated with the express channels. In such an application, the two factors limiting the maximum number of cascable nodes are the pass band (amplitude response) and the group delay (phase response). As the data rate increases, the system becomes more sensitive to variations in dispersion within the signal bandwidth. Accordingly, the linear phase is a crucial parameter in determining the useable effective pass band in 40 Gb/s systems.

From the original concept of the digital filter and interleaver structure, just like the minimum phase filter and the maximum phase filter, the opposite slopes of the dispersion from the opposite paths showed in Fig 2.10.

And the corresponding delay characteristic is showed in the figure 3.1

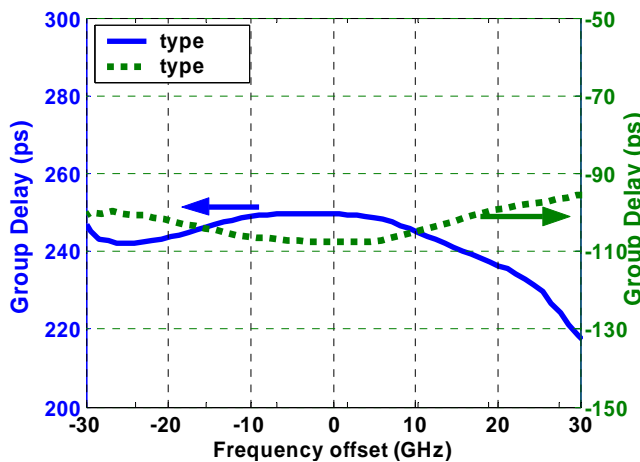


Fig. 3.1 In-band group delay for two types of interleaver connection

With two mirrored group delay characteristics, the induced dispersion by an interleaver can be compensated with proper connection of interleaver pair, showed as

Figure 3.2. Clearly, for the compensated connection, the induced in-band dispersion is insignificant comparing with the uncompensation case (showed in figure 3.3). Figure 3.4 shows the accumulated transmission spectrum and group delay after cascading five interleaver pairs by computer simulation.

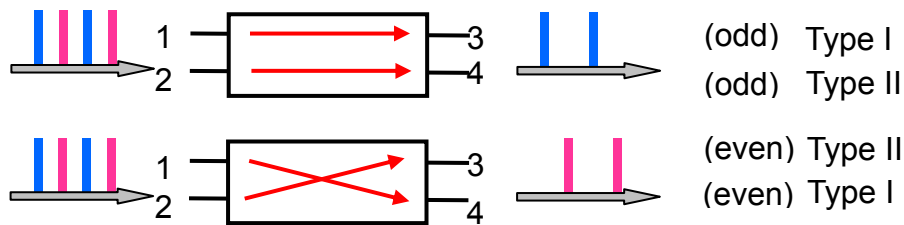


Fig. 3.2. Passband of the interleaver for even and odd channel

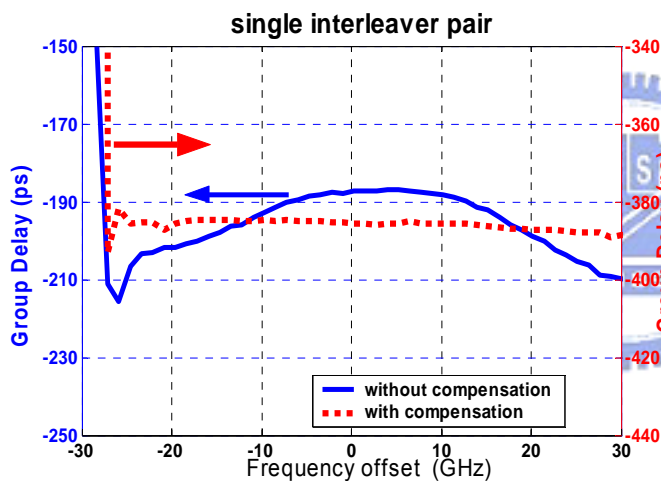


Fig. 3.3 group delays curve of compensated and uncompensated interleaver-pair connection

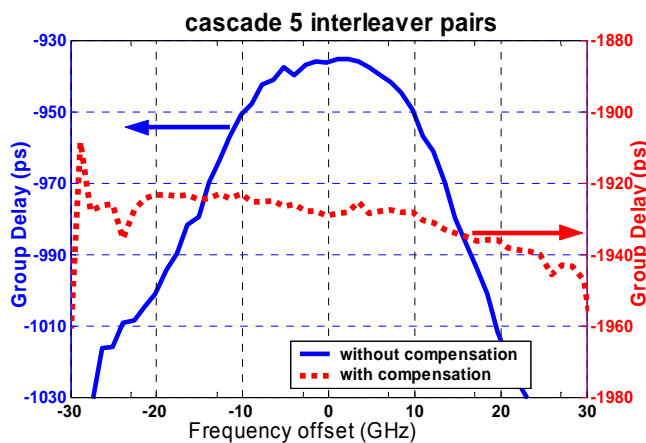


Fig. 3.4 the accumulated transmission spectrum and group delay curves after cascading five interleaver pairs.

Clearly, the accumulated group delay is less than 20 ps in the passband. However, the accumulated group delay is over 60 ps.

3.2 Re-circulating loop transmission

A circulating loop transmission experiment is a useful tool for the research and development of long-haul transmission systems that use Erbium-doped fiber-amplifier repeaters. Circulating loop techniques, applied to an amplifier chain of modest length, can provide an experimental platform to study a broad range of transmission phenomena for EDFA-based transmission systems. Optical loop configurations allow designers to simulate long haul optical transmission system with just a fraction of the overall system hardware (fiber, optical amplifiers, filters, etc.). The designer benefits from reduced setup size, complexity, and cost. Circulating loop experiments yield valuable information on the full system BER, eye diagram shape, dispersion, signal-to-noise ratio, and interchannel interaction of a WDM system.

The loop experiment contains most of the same elements typically found in conventional experiments, such as an optical data transmitter/regenerator pair, a chain of amplifier/fiber sections, and diagnostic equipment such as a bit error test set (BERTS) (Fig 3.5). In the loop experiment, optical switch is added to allow data to flow into the loop (the load state) or to allow data to circulate (the loop state), Fig 3.6.

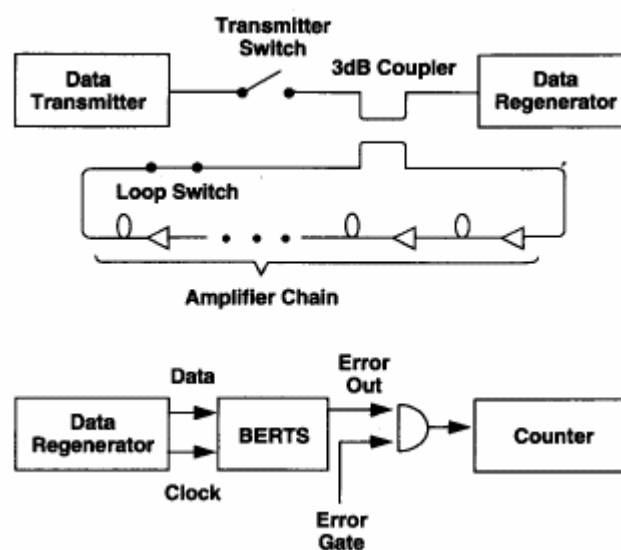


Fig. 3.5. loop transmission block diagram

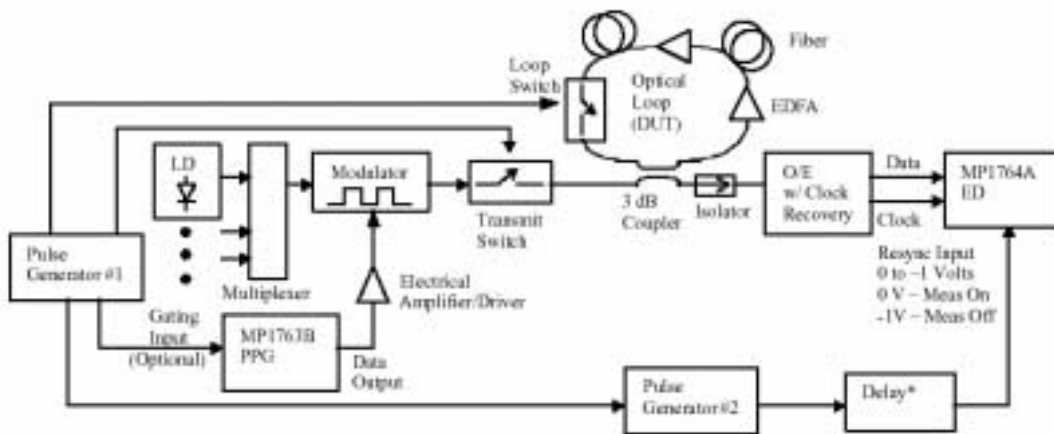


Fig. 3.6. (a) load state (b) loop state

The basic time unit for the experiment is the round trip time of the closed loop time, calculated by the given refraction index of the transmission fiber in the loop.

3.3 Key components & techniques of the loop experiment

Figure 3.7 shows the conceptual circulating loop setup.



*A separate Delay circuit is not required if Pulse Generator #2 has a "Trigger Delay" feature.

Fig. 3.7. circulating loop setup

There are some key components of loop experiment as listed below.

Optical loop: The optical loop consists of representative portion of the overall transmission system. Typically, the loop contains spans of fiber separated by optical amplifiers/isolator/filters. The minimum length of the loop (minimum loop time) is constrained by the sync time of the Error Detector. The typical value of sync time for 10 Gb/s bit rate is approximately 1 us. However, the maximum length of the loop is limited only by the user's resource. The round trip gain of the loop must be adjusted to equal 1. This allows the data to re-circulate without loss.

Pulse generator #1: provide synchronizing signals to the loop switch, transmit switch,

pulse pattern generator, and pulse generator #2. The pulse width of PG#1, t , is derived from the loop time. The period, P , is dependent on the maximum simulated distance.

Pulse generator #2: this pulse generator is slaved to pulse generator #1. The pulse width setting of this unit is slightly less than t to account for traveling edge switching transients. The traveling edge transient time is related to the fall time of the transmit switch. It's recommended that the Pulse width of pulse generator #2 be 2 us less than t .

Transmit switch/loop switch: these switch must have low insertion loss, low polarization dependency, high extinction ratio, and small rise/fall times to minimize transient. The repetition rate of the switch is a function of the loop time. Typical repetition rates are in the kHz range.

O/E with Clock Recovery: This circuit converts the Optical Loop output signal to electrical DATA and CLOCK signals suitable for input into the Error Detector. The voltage levels into the Error Detector should be in the range 0.25 to 2.0 Vp-p (this is guaranteed input range; ED typically work properly for input levels down to 50 mVp-p).

Pulse Pattern Generator: The PPG provides the gigabit bit pattern that drives the optical modulator. The PPG data output must produce a high quality eye diagram, i.e. fast rise/fall times, low distortion, low jitter, and high Q factor² (minimal noise on the eye "rails"). The Anritsu MP1763B has a tr/ta of 30 ps, less than 10% distortion, 20 ps p-p of crossover jitter, and a Q factor of >40.

Error Detector: The ED must be able to synchronize quickly on incoming burst data. An Error Detector cannot make valid error measurements until synchronization is achieved. Circulating Loop tests are not possible if the sync time approaches or exceeds the duration of the burst data. The Anritsu MP1764A has very fast synchronization times for both standard PRBS patterns and user defined patterns

(DATA).

LD, multiplexer, modulator, and electrical amplifier: the LD is typical a DFB operating in the 1550 nm or 1310 nm window. Multiple 1550 nm band DFB source can be used in conjunction with a multiplexer to simulate WDM channels. Each DFB is modulated directly with Lithium Niobate or EOM modulator.

3.3.1 Dispersion management

For long-haul transmission systems, the nonlinear refractive index can couple different signal channels, and can also couple the signal with noise. It will cause the distortion, spectrum broadening and other degradations. If it is operated around the zero dispersion wavelength in fiber, the data signals and the amplifier noise with wavelengths similar to the signal travel at similar velocity. Under these conditions the signal and noise waves have long interaction lengths and can mix together. Especially the NRZ format is affected severely by nonlinearity because it has long interaction lengths. Chromatic dispersion causes different wavelengths to travel at different group velocities in single mode transmission fiber. Chromatic dispersion can reduce phase matching, or the propagation distance over which closely spaced wavelengths overlap, and can reduce the amount of nonlinear interaction in the fiber. Thus, in a long undersea system, the nonlinear behavior can be managed by tailoring the accumulated dispersion so that the phase-matching lengths are short, and the end-to-end dispersion is small. The technique has been used in both single channel systems to reduce nonlinear interaction between signal and noise as well as in WDM system.

A special kind of fiber, known as the dispersion-compensating fiber (DCF), has been developed to reduce the accumulated dispersion. The use of DCF provides an all optical technique that is capable of compensating the fiber GVD completely if the average optical power is kept low enough that the nonlinear effects inside optical fibers are negligible. It takes advantage of the linear nature of the pulse-propagation

Equation: $\frac{\partial A}{\partial Z} + \frac{i\beta_2}{2} \frac{\partial^2 A}{\partial t^2} - \frac{\beta_3}{6} \frac{\partial^3 A}{\partial t^3} = 0$, where A is the pulse-envelope amplitude.

The effects of third-order dispersion are included by the β_3 term. In practice, this term can be neglected when $|\beta_2|$ exceeds $0.1 \text{ ps}^2/\text{km}$.

There are two kinds of fiber in the optical loop: Corning LEAF and Corning DCF. The length of the DCF is designed to fully compensate the dispersion induced by the LEAF (at **193.20Thz**) . The corresponding parameters are listed below:

- Dispersion of Leaf: 4.1689 at 1553.33nm
- Dispersion of DCF: -86.6231 at 1553.33nm
- Leaf length= 25 km ;
- DCF length=4.18km;
- Leaf length= 75 km ;

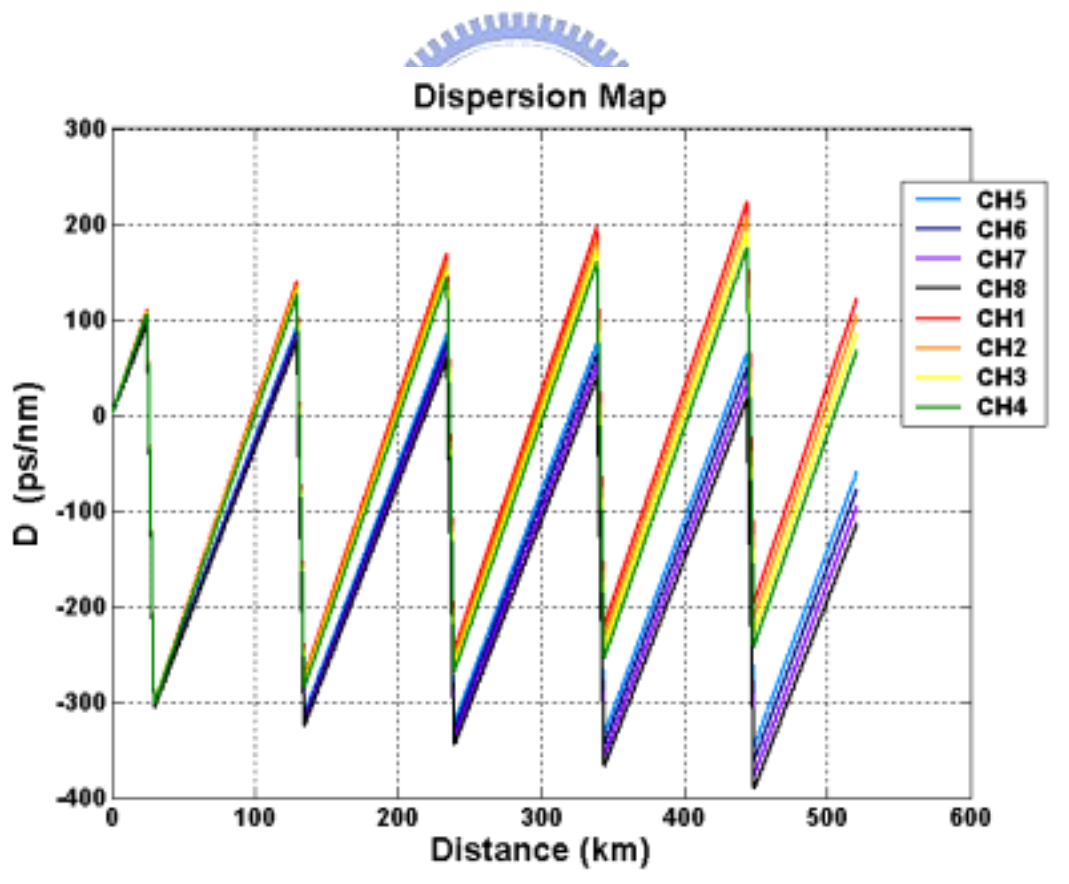


Fig. 3.8. Dispersion map (fully compensated in 193.2THz)

3.3.2 Loop time control

The basic time unit for the experiment is the round-trip time of the closed loop (shown in Fig. 3.9). With reference to the timing diagram Fig. 3.6 (a), the experiment starts with the transmitter switch on and the loop switch off.

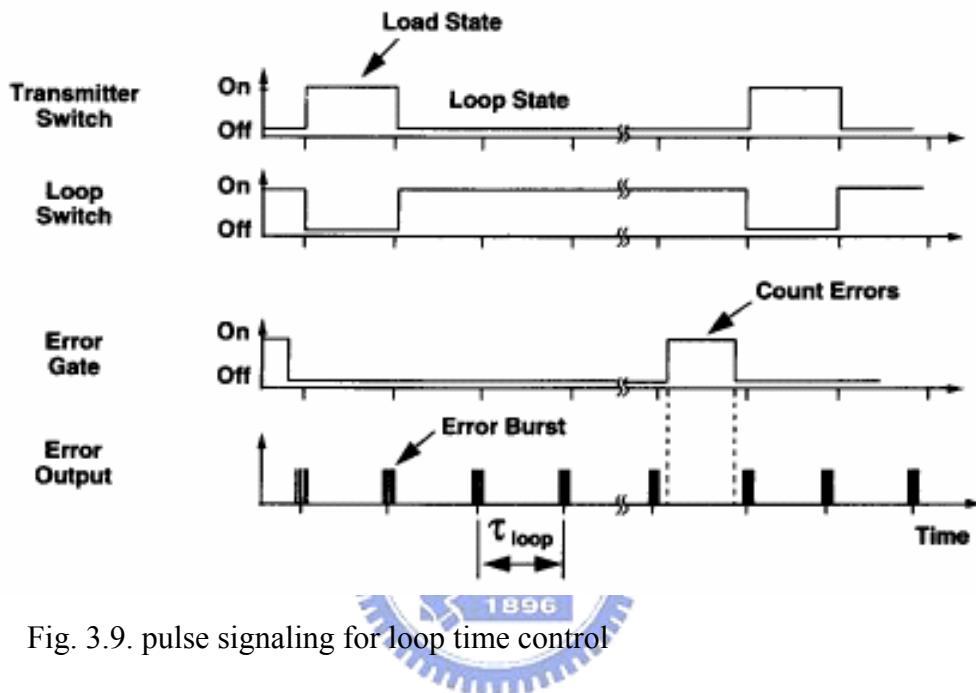


Fig. 3.9. pulse signaling for loop time control

The two switches are held in this load state for at least one loop time to fill the loop with the optical signals. Once the loop is loaded with data, the switches change state to the loop state as Fig. 3.6 (b), and the data is allowed to circulate around the loop for some specified number of revolutions. A portion of the data signals are coupled to the receiver for analysis. The data signals are received and re-timed by the receiver and compared to the transmitted signal in the BERTS for error detection. The error signals from the BERTS are combined with the error gate in a logic AND gate so that only the errors in the last circulation are counted. The measurement continues, switching between the load and loop states so that errors can be accumulated over long intervals of time. The BER is calculated as the number of

errors detected in the error gate period divided by the total number of bits transmitted during the observation period.

With an unbroken data pattern, the BERTS still detects errors at the boundaries between each loop time, related to the finite speed of the AO switches. During the switch transition from the load state to the loop state, both switches are transmitting some amount of the optical signal. Optical pulses originating from the transmitter will interfere with those pulses returning from the loop, since two pulses have the same wavelength, but random optical phase and polarization. This interference process corrupts the data bits and causes the BERTS to detect bit errors at the transitions.

The circulating loop experiment can be improved upon through the use of bit error detectors with fast frame synchronization time (usually referred to as “burst mode”). Because the frame synchronization time of these detectors is much shorter than the loop time, they simplify error counting by de-coupling the strict relationship between the bit rate and the loop time, thus allowing the transmitter to run asynchronous to the loop. Here, the receiver sees broken sections of the transmitted pattern at each circulation because the data words do not fit evenly into the loop. At each border between circulations, the error detector must re-acquire frame synchronization, thus creating a small error burst on the seam. As in the control scheme discussed above, this error burst is removed by gating the error detector and counting only those errors that occur in the middle of the circulation.

3.3.3 Setup & results

Many DWDM systems have used interleavers as multiplexers and de-multiplexers. In a metro system, a pair of interleavers can be used in add/drop applications to provide up to 50% adding and dropping of total traffic while

simultaneously reducing the insertion loss associated with the express channels. In such an application, the two factors limiting the maximum number of cascaded nodes are the pass band (amplitude response) and the group delay (phase response). As the data rate increases, the system becomes more sensitive to variations in dispersion within the signal bandwidth. Accordingly, the linear phase is a crucial parameter in determining the useable effective pass band in 40 Gb/s systems.

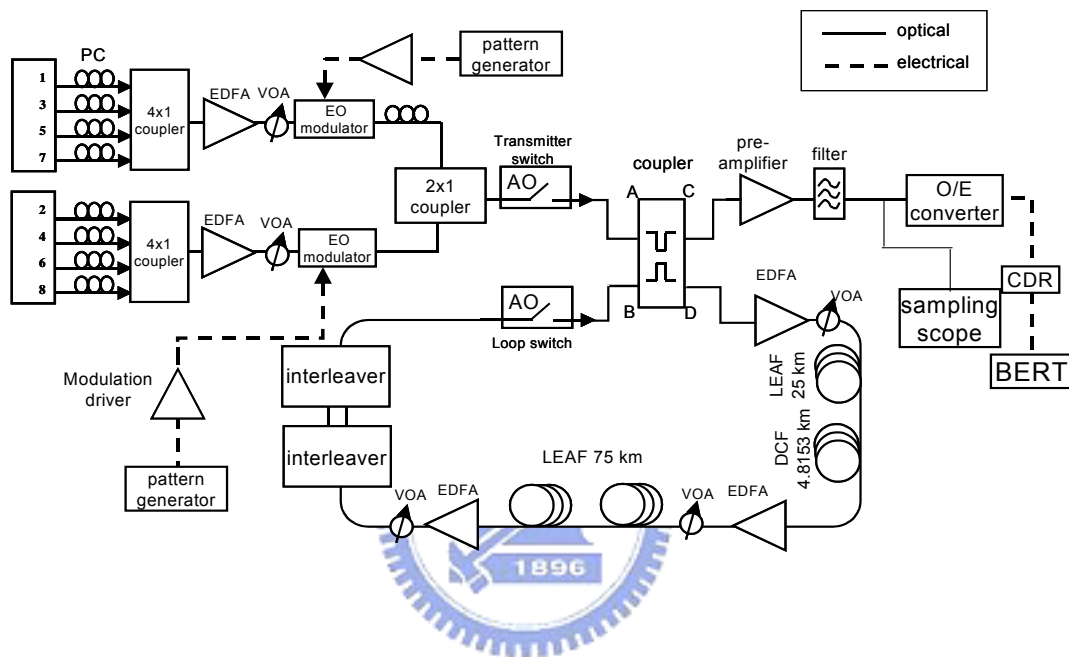
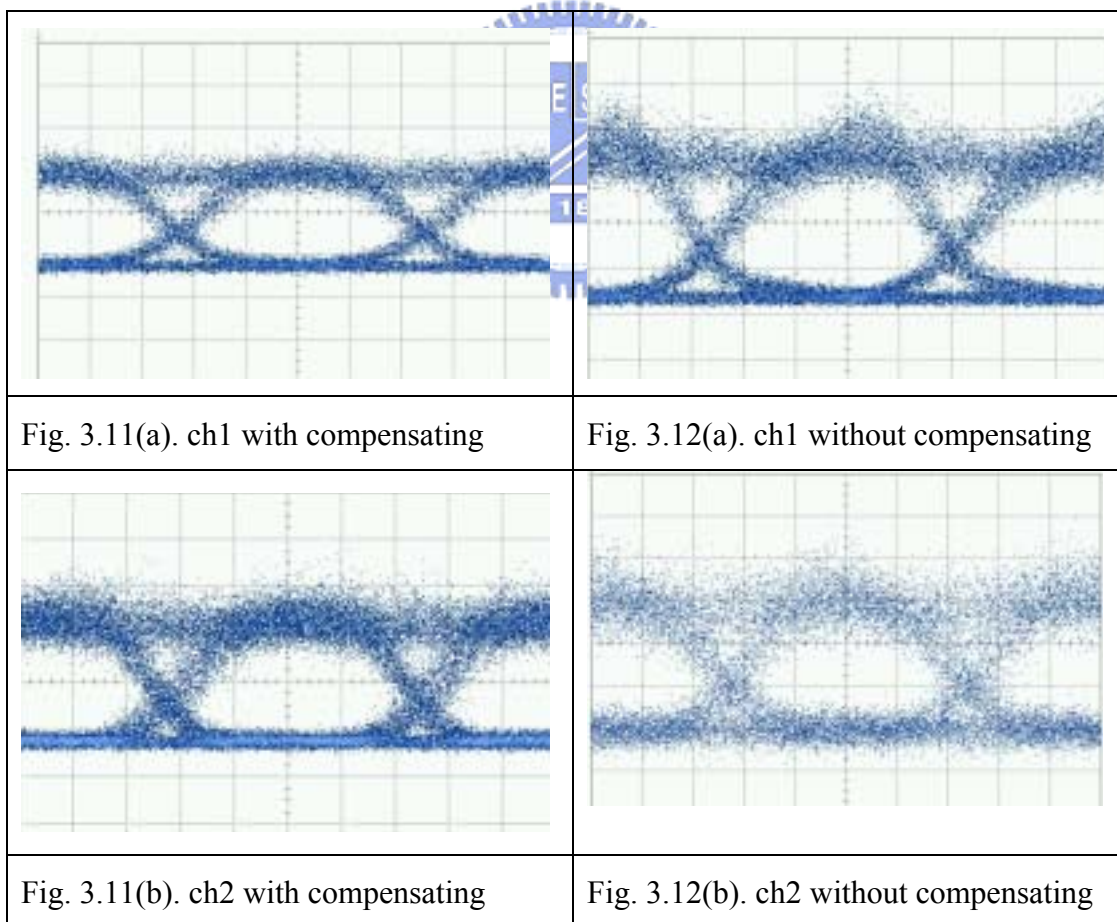


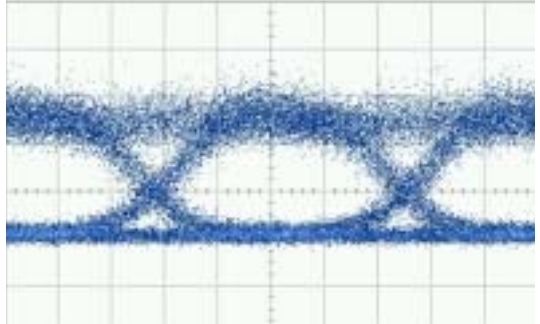
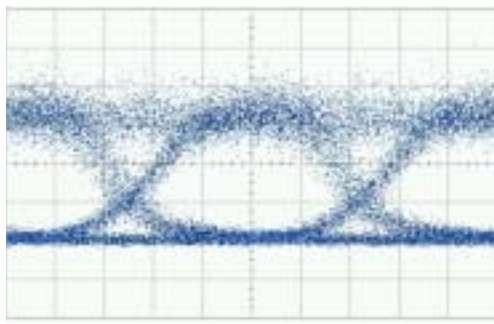
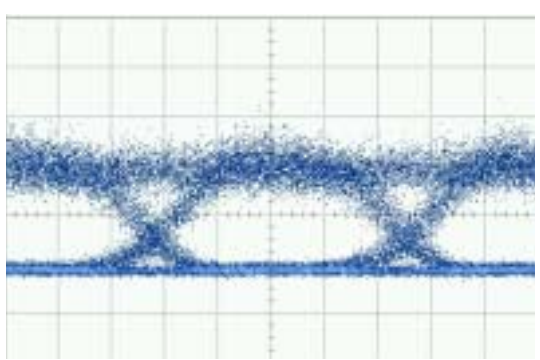
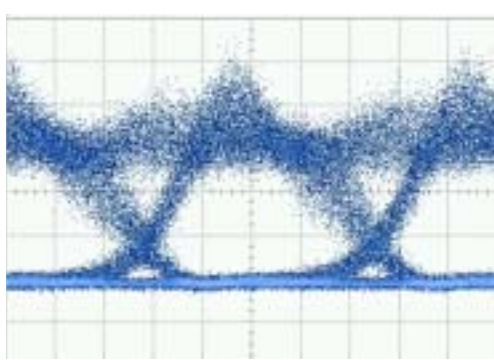
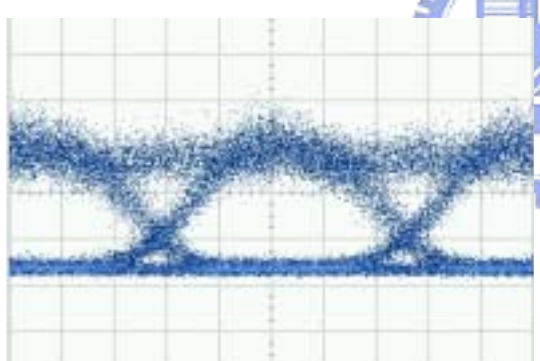
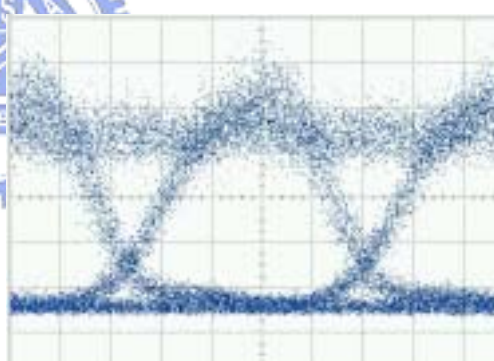
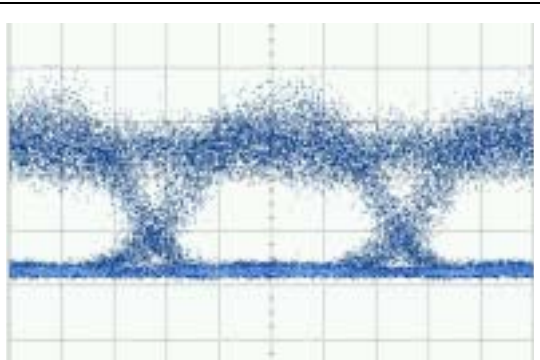
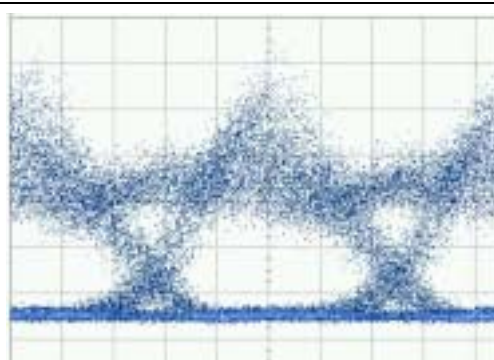
Fig. 3.10. circulating loop setup

To demonstrate the feasibility of cascading the interleaver pairs, a re-circulating loop was employed to simulate multiple adds/drops in a ring network. Figure 3.10 shows the experimental setup of the re-circulating loop. The eight-channel laser sources consist of two groups: one group from 193.2 THz to 193.35 THz and the other one from 192.7 THz to 192.85 THz; all with 50-GHz channel spacing. The odd channels and even channels were individually modulated by a LiNbO₃ EO modulator at 10 Gb/s with pseudo random binary sequence (PRBS) length of $2^{31}-1$ patterns. A polarization controller is used to set the polarization state of the odd channels to being orthogonal to that of the even channels to reduce the deleterious nonlinear effects.

Two types of fiber were used in the re-circulating loop: 100-km of Corning LEAF fiber and 4.8-km of Corning DCF for compensating the accumulated chromatic dispersion in LEAF fiber. The fully-compensated wavelength of this fiber loop was located at 1552 nm. After 105-km of fiber, the interleaver pair was inserted in the fiber loop to simulate optical channels add/drop at every 105 km. A 3R receiver of -33 -dBm sensitivity at BER equals to 10^{-9} was used to detect the signal's performance after transmission.

Figure 3.11 (a)~(h) shows the corresponding eye patterns with compensating connection, and Figure 3.12 (a)~(h) are those without compensating connection



	
<p>Fig. 3.11(c). ch3 with compensating</p>	<p>Fig. 3.12(c). ch3 without compensating</p>
	
<p>Fig. 3.11(d). ch4 with compensating</p>	<p>Fig. 3.12(d). ch4 without compensating</p>
	
<p>Fig. 3.11(e). ch5 with compensating</p>	<p>Fig. 3.12(e). ch5 without compensating</p>
	
<p>Fig. 3.11(f). ch6 with compensating</p>	<p>Fig. 3.12(f). ch6 without compensating</p>

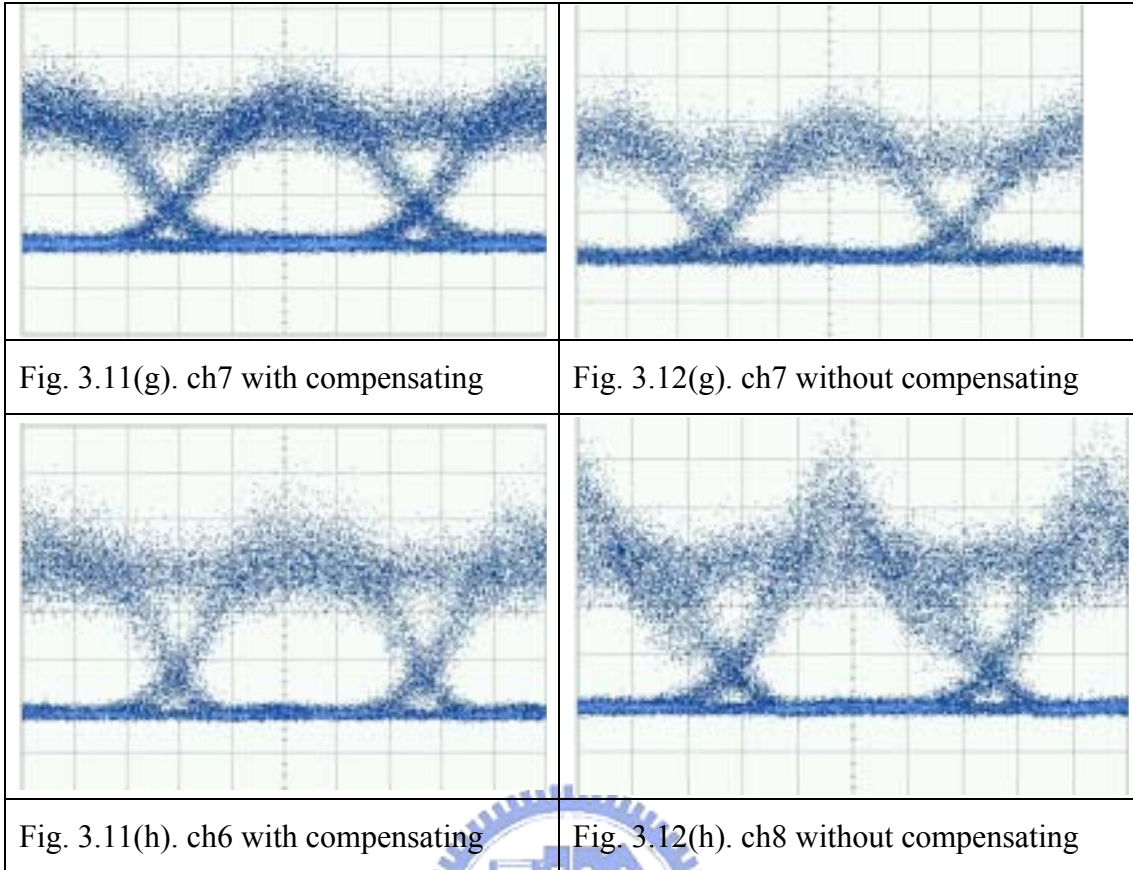


Figure 3.13 shows the receiving sensitivity at BER equals to 10^{-9} of each channel after five loops, i.e., about 500-km of transmission and five times of add/drop by the interleaver pairs, for both compensated and uncompensated cases. Since the two groups of channels were intentionally selected to locate at the wavelength regions with opposite sign of dispersion: one with negative dispersion, and the other one with positive dispersion, the experimental results for both cases indicate that the receiving sensitivities of eight-channels exhibit a parabolic distribution centered at dispersion-zero wavelength. The difference of sensitivity is insignificant between the two cases. This is because, as the channel wavelengths are set at the center of the interleaver's pass band precisely, there's negligible dispersion introduced by the interleaver, even for the uncompensated case.

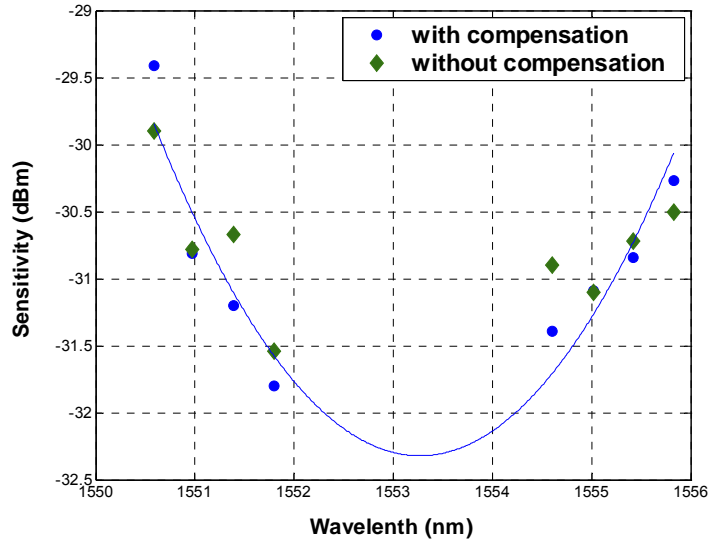


Fig. 3.13. Receiving sensitivity for compensated and uncompensated after cascaded five interleaver-pairs

However, if the channel wavelength does not coincide with the ITU grids, a significant dispersion is introduced in the uncompensated case. Figure 4 shows the BER curves and the corresponding eye diagrams when wavelength is either on the ITU grid or detuned from the ITU wavelength by ± 0.07 nm at channel five. Figure 3.14 (a) demonstrates the experimental results for the uncompensated case and Figure 3.14 (b) depicts for the compensated case. Figure 3.14 (a) shows that a considerable performance differential, of more than 2.5 dB sensitivity power penalty, was observed after detuning the wavelength from the ITU grid. When the wavelength was detuned by $+ 0.07$ nm, a 1.5-dB sensitivity improvement is obtained because the interleaver-induced dispersion can further compensates the accumulated residual dispersion at channel five. A better eye diagram also indicates the improvement. Furthermore, the receiving sensitivity is even better than those of the compensated cases by 1 dB. However, when the wavelength was detuned by $- 0.07$ nm, since the interleaver-induced dispersion has the same sign as the residual dispersion, the performance was further degraded. However, in Figure 3.14 (b), the BER curves

and eye diagrams show no significant difference after the wavelength is detuned by ± 0.07 nm at the same channel, since the dispersion introduced by the compensated interleaver pair was negligible.

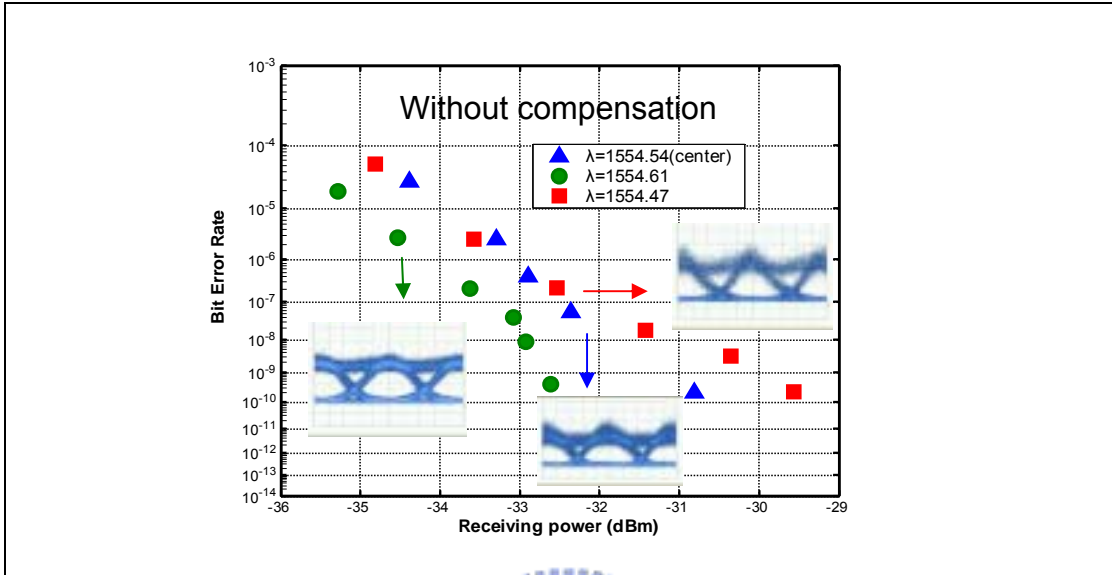


Fig. 3.14 (a). BER curves and corresponding eye diagrams at channel five when wavelength is detuned without compensation connection

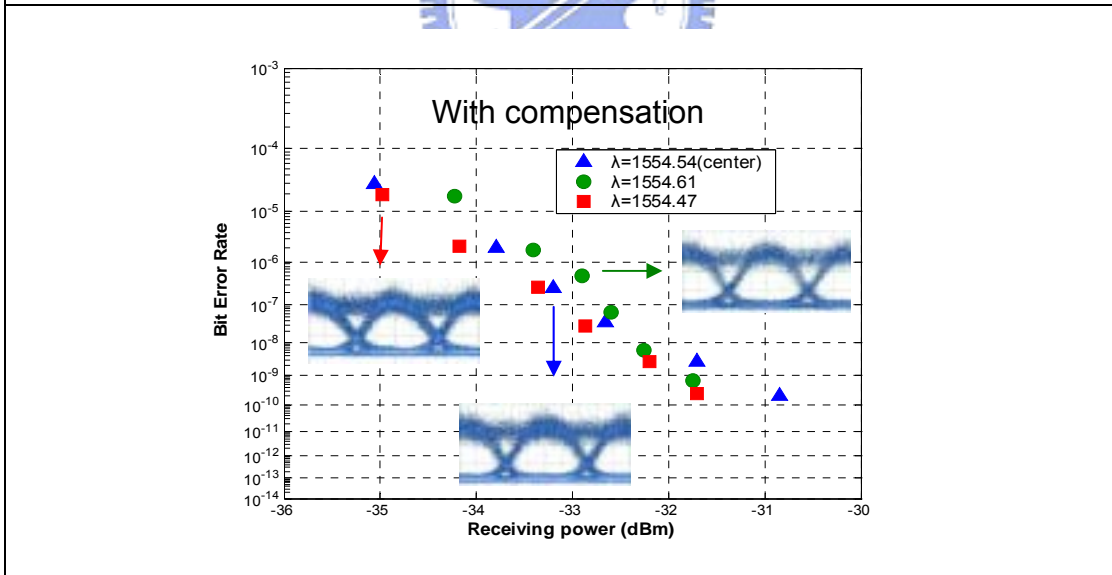


Fig. 3.14 (b). BER curves and corresponding eye diagrams at channel five when wavelength is detuned with compensation connection

References

- [3.1] Bergano, N. S, C. R. Davidson, Circulating Loop Experiments for the Study of Long-Haul Transmission Systems Using Erbium-Doped Fiber Amplifiers, *Journal of Lightwave Technology*, Vol. 13, No. 5, May 1995
- [3.2] Bergano, N. S., F. W. Kerfoot, and C. R. Davidson, Margin Measurements in Optical Amplifier Systems, *IEEE Photonics Technology Letters*, Vol. 5, No 3, March 1993.
- [3.3] Application Note of **Anritsu MP1764A 12.5 Ghz Error Detector**
- [3.4] Masataka Nakazawa, *Fellow, IEEE*, Solitons for Breaking Barriers to Terabit/Second WDM and OTDM Transmission in the Next Millennium, *IEEE JOURNAL ON SELECTED TOPICS IN QUANTUM ELECTRONICS*, VOL. 6, NO. 6, NOVEMBER/DECEMBER 2000
- [3.5] P. C. Becker and N. A. Olsson, “Erbium-Doped Fiber Amplifiers Fundamentals and Technology,” New York: Academic, 1999.



Chapter 4

Bidirectional transmission experiment

4.1 Bidirectional Add/Drop Amplifier (BADA)

Wavelength-division-multiplexing (WDM) add/drop multiplexer (ADM) is one of the key elements to implement a WDM self-healing ring (SHR) network. Previously, WDM SHR networks have been demonstrated by using unidirectional W-ADM. However, these networks would require four fiber links: two fiber links each for the working and protection rings. The number of these fiber links could be halved by using the bidirectional W-ADM instead of unidirectional W-ADM.

In bidirectional networks employing optical amplifiers, if signals are bidirectionally transmitted over a single fiber path, optical isolators cannot be used to prevent multiple reflections that can significantly degrade the receiver sensitivity. Therefore, system performances are severely degraded due to multiple reflections. It has been observed that due to multiple reflections along a fiber path, the laser phase noise is converted to the intensity noise, which may cause performance degradations in high-speed lightwave systems. Even if discrete reflections are carefully suppressed by using nonreflective connector facets, the multiple Rayleigh backscattering (RB) in fibers gives rise to the phase-to-intensity noise conversion.

While interleaved bidirectional transmissions (figure 4.1) offer effective means for four-wave mixing (FWM) suppression, they generate the coherent (in-band) crosstalk and incoherent (out-of-band) crosstalk at an amplification node (figure 4.2). Even for a case of non-reflective connector facets, in- and out-of-band crosstalk is generated by intra-span Rayleigh backscatter (RB). In-band (coherent) crosstalk is generated by completing double reflective pass (solid line), producing the term $P_x^{WE} = P^{WE} G^2 R^2$, where G is the amplifier gain and R is RB level. Similarly,

out-of-band crosstalk generated by a single RB (dashed line in Fig 4.2), has a level of $P_x^{EW} = P^{EW} GR$. Combination of a typical RB level (32 dB) and 24-dB amplifier gain generates levels of in- and out-of-band crosstalk at 16 dB and 8 dB, respectively. In addition, bidirectional amplifier node is susceptible to occurrences of self-oscillation; distributed Rayleigh mirrors are forming optical cavity with enclosed amplifier gain, thus, providing necessary conditions for node lasing. Careful design of bidirectional node, therefore, requires suppression of round-trip gain not only within the transmission window, but across the entire gain spectrum of the amplifier.

Most of BADA employed two unidirectional optical amplifiers (UOAs) together with optical circulators or WDM filters to separate the signals propagating in the opposite directions. And their performance has been greatly improved by suppressing the relative intensity noise due to Rayleigh backscattering and optical reflections and removing amplified spontaneous emission (ASE) noise from the Er-doped fiber amplifier (EDFA) using the bandpass filters or fiber Bragg gratings. However, those repeaters tend to be costly because EDFAs, circulators, WDM filters, and other accessories are expensive. This hinders the bidirectional WDM transmission systems to penetrate deep into the metro and access networks whose traffic is rapidly growing due to the Internet.

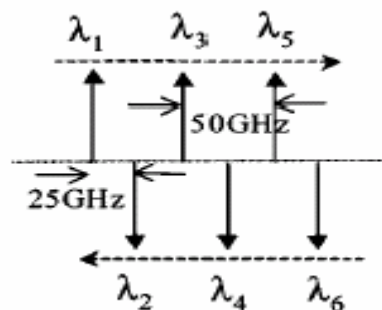


Fig. 4.1 interleaved bidirectional path plan

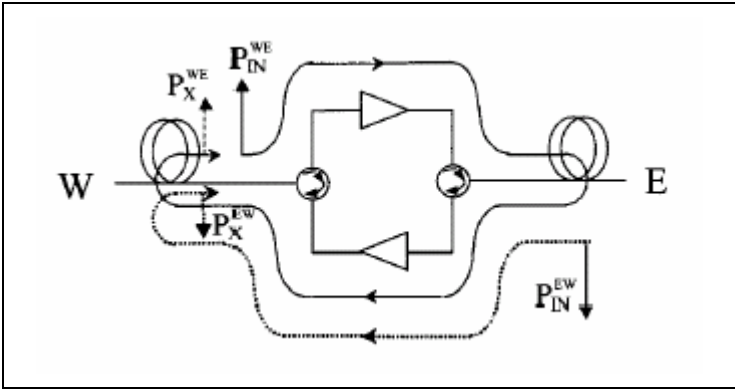


Fig. 4.2 In- and out-of-band crosstalk in bidirectional transmission systems.

4.2 Non-linear effects

The response of any dielectric to light becomes nonlinear for intense electromagnetic fields, and optical fiber are no exception. On a fundamental level, the origin of nonlinear response is related to anharmonic motion of bond electrons under the influence of an applied field. As a result, the induced polarization P from the electric dipoles is not linear in the electric field E , but satisfies the more general relation $P = \epsilon_0 \{ \chi^{(1)} \cdot E + \chi^{(2)} : EE + \chi^{(3)} : EEE + \dots \}$, where ϵ_0 is the vacuum permittivity and $\chi^{(j)}$ ($j=1,2,3,\dots$) is j th order susceptibility. To account for the light polarization effects, $\chi^{(j)}$ is a tensor of rank $j+1$. The linear susceptibility $\chi^{(1)}$ represents the dominant contribution to P . Its effects are included through the refractive index n and the attenuation coefficient α .

The nonlinear effects governed by the third-order susceptibility $\chi^{(3)}$ are elastic in the sense that no energy is exchanged between the electromagnetic field and the dielectric medium. Thus, a second class of nonlinear effects results from stimulated inelastic scattering in which the optical field transfers part of its energy to the nonlinear medium. Two important nonlinear effects in optical fiber fall in this category; both of them are related to vibrational excitation mode of silica. These two phenomena are known as stimulated Raman scattering (SRS) and stimulated Brillouin

scattering. The fundamental difference is that SBS in optical fiber occurs only in the backward direction whereas SRS dominates in the forward direction. Another nonlinear effect called Rayleigh backscattering (RB) will also degrade the bidirectional transmission system. Because any backward scattering will interfere the backward signal directly, so I'll focus on SBS and RB effects in the next two sections.

4.2.1 Stimulated Brillouin scattering

Stimulated Brillouin scattering is a nonlinear process that can occur in optical fiber at input power levels much lower than those needed for stimulated Raman scattering (SRS). It manifests through the generation of a backward-propagating Stoke wave that carries most of the input energy, once the Brillouin threshold is reached. SBS can be detrimental for optical communication systems. The threshold pump power for SBS depends on the spectral width associated with the pump wave. It can be as low as $\sim 1\text{mW}$ for a cw pump or for relatively wide pump pulses (width $> 1\mu\text{s}$). By contrast, SBS nearly ceases to occur for short pump pulses with width $< 10\text{ns}$.

The process of SBS can be described classically as a parametric interaction among the pump wave, the Stokes wave, and an acoustic wave. The pump wave generates acoustic waves through the process of electrostriction which in turn causes a periodic modulation of the refractive index. The pump-induced index grating scatters the pump light through Bragg diffraction. Scattered light is down-shift in frequency because of the Doppler shift associated with a grating moving at the acoustic velocity v_A . Since both the energy and the momentum must be conserved during each scattering event, the frequency and the wave vectors of the three waves are related by:

$$\begin{aligned} \omega_A &= \omega_p - \omega_s \\ \kappa_A &= \kappa_p - \kappa_s \end{aligned}, \text{(Eq 4.1)}$$

Where ω_p and ω_s are the frequencies and κ_p and κ_s are the wave vectors of the pump and Stokes waves, respectively. The frequency ω_A and the wave vector κ_A of the acoustic wave satisfy the dispersion relation:

$$\omega_A = |\kappa_A| v_A = 2v_A |\kappa_p| \sin(\theta/2), \quad (\text{Eq. 4.2})$$

, where θ is the angle between the pump and Stokes waves, and the vector relation (4.1)

was used while $|\kappa_p| = |\kappa_s|$. Equation (4.2) shows that frequency shift of Stokes wave

depends on the scattering angle. In particular, it is maximum in the backward

direction ($\theta=\pi$) and vanishes in the forward direction ($\theta=0$). The frequency shift ν_B in

the backward direction is given by

$$\nu_B = \frac{\omega_A}{2\pi} = \frac{2n v_A}{\lambda_p}, \quad (\text{Eq. 4.3}),$$

where Equation (4.2) was used with $|\kappa_p| = \frac{2\pi}{\lambda_p}$, n is the refractive index, and λ_p is the pump wavelength.

In a single mode optical fiber, the only relevant directions are the forward and backward directions. Even though Equation (4.2) predicts that Brillouin scattering should not occur in the forward direction ($\theta=0$), spontaneous or thermal Brillouin scattering in the forward direction can occur in optical fiber. This happens because the guided nature of acoustic waves leads to a relaxation of the wave-vector selection rule. As a result, a small amount of Stokes light is generated in the forward direction. This phenomenon is referred to as guided acoustic-wave Brillouin scattering. Because of its extremely weak character, this phenomenon is not considered further. SBS in optical fibers occurs only in the backward direction with Brillouin shift given by Equation (4.3). If we use $v_A=5.96$ km/s and $n=1.45$, the value appropriate for silica fibers, $\nu_B \cong 1.11$ GHz at $\lambda_p=1.55\mu\text{m}$.

In order to reduce Brillouin scattering, we control the total optical power under

6dBm while propagating through fiber.

4.2.2 Rayleigh backscattering

Refractive-index variations arisen from compositional fluctuations occurring during drawing fibers give rise to RB. For the analysis of backscattered signals, a two-dimensional (2-D) fiber model was used in Fig. 4.3. A fiber with the L is divided by N_s scatter sections, and $\Delta L = L / N_s$ is the scatter section length.

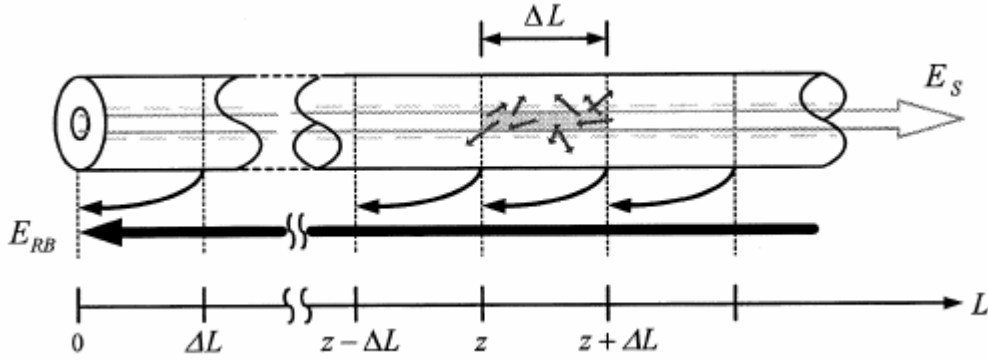


Fig. 4.3. Schematic of modeling Rayleigh backscattering in fiber. The light scattered from each section travels back to the beginning point and sums up.

A linearly polarized electrical field of the transmitted signal is given by its complex amplitude vector :

$$\begin{aligned} \vec{e}_s(t, z) &= \vec{E}_s(t, z) \exp[j\omega_0 t] \\ \vec{E}_s(t, z) &= \vec{p}_s S_s(t, z) \exp[j\phi(t)] \end{aligned} \quad , \text{ (Eq 4.4),}$$

where the Jones vector \vec{p}_s indicates the state of polarization of the field, \vec{E}_s is the field envelope, ω_0 is the optical carrier frequency, and $\phi(t)$ describes the phase noise of transmitter outputs. If we define the fraction of the scattered field from a section located at z , which is guided in the backward direction as the backscattering coefficient $\Delta\rho(z)$, the backscattered signal $\Delta\vec{E}_b(t, z)$ arrived at the fiber input facet from a scatter section located at is given by

$$\Delta\vec{E}_b(t, z) = M(z) \vec{E}_s\left(t - \frac{2z}{v_g}\right) \exp\left[-\left(\frac{\alpha}{2} + j\beta\right) \cdot 2z\right] \Delta\rho(z) \quad , \text{ (Eq 4.5),}$$

with the fiber attenuation coefficient α , the group velocity v_g , and the propagating constant β . The unitary Jones matrix $M(z)$ describes the change of the polarization state of the electric field propagating along the axis. Therefore, the total backscattered field at the fiber input facet is the superposition of the field contributions from each scatter section

$$\vec{E}_b(t) = \sum_{n_s=1}^{N_s} \Delta \vec{E}_b(t, n_s, \Delta L) \quad , \text{(Eq 4.5)}$$

Using the differential backscattering coefficient, the mean backscattered intensity is given by

$$\begin{aligned} \langle I_b \rangle &= \iint_{0 \ 0}^L \left\langle (M(z_1) \vec{E}_s(t - 2z_1 / v_g))^c \cdot (M(z_2) \vec{E}_s(t - 2z_2 / v_g)) \cdot \rho^*(z_1) \rho(z_1) \right\rangle \\ &\quad \cdot e^{-\alpha(z_1+z_2)} \cdot e^{j2\beta(z_1-z_2)} dz_1 dz_2 \\ &= 2\sigma^2 I_s (1 - e^{-2\alpha L}) / 2\alpha = \frac{S\alpha_s}{2\alpha} \cdot (1 - e^{-2\alpha L}) \cdot I_s, R_{bs} = \frac{S\alpha_s}{2\alpha} \cdot (1 - e^{-2\alpha L}) \quad , \text{(Eq 4.6)} \end{aligned}$$

,where I_s is source intensity, σ^2 is the variance of $\rho(z)$, α_s is the attenuation coefficient due to Rayleigh scattering, S is the recapture factor, and R_{bs} denotes the intensity RB coefficient. Recapture factor S is the fraction of the total Rayleigh-scattered power that gets captured in the fiber and propagates in the backward direction. The RB level converges to the mean value $\langle I_b \rangle$ as the scatter section length equal to the minimum fiber length W ($W = \lim_{N_s \rightarrow \infty} L / N_s$, where we assumed that N_s is a enormous figure numerically). We can use the constant RB coefficient to model RB, regardless of pulse patterns.

The RB coefficient is typically obtained in the range from -31 to -34 dB for a single-mode fiber (SMF) at $1.55 \mu m$. However, for the bidirectional transmission systems with EDFAs for inline optical amplifiers, the Rayleigh backscattered signal counter-propagates through optical amplifiers, so the effective RB coefficient

becomes GR_{bs} . These non-negligible effective RB terms degrade the system severely. The single-amplified Rayleigh backscattered signal is backscattered again at the opposite side and counterpropagates through optical amplifiers, so the double-amplified Rayleigh backscattered signal copropagates with the transmitted signals. The presence of double-amplified RB causes the relative intensity noise (RIN) produced by the interference between transmitted signals. In the same way, both single-amplified RB (GR_{bs}) and double-amplified RB ($G^2R_{bs}^2$) of the amplified spontaneous emission (ASE) noise increase the total received ASE power at receiver and, thus, are important elements in determining the noise characteristics. To clarify, Fig. 4.4 shows these different backscattering cases with the effective RB coefficient.

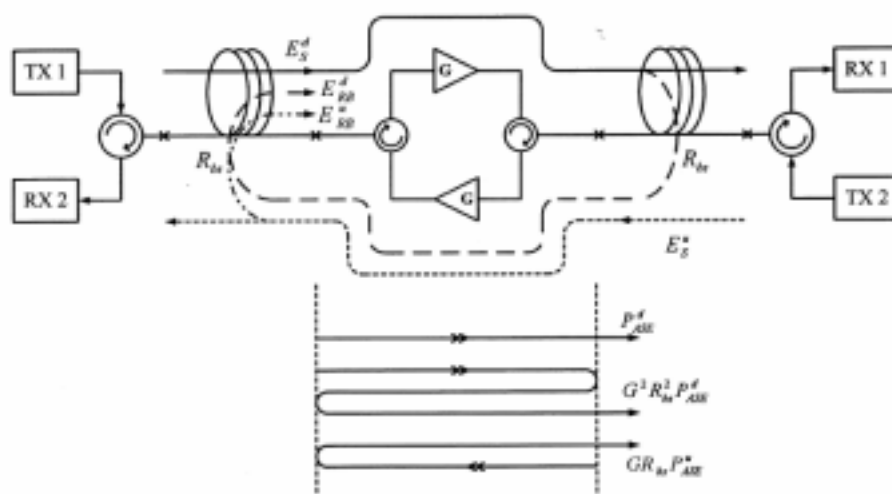


Fig. 4.4. Scheme of crosstalk due to single- and double-amplified RB of signal as well as ASE. P_{ASE} is the power of ASE noise from the EDFA. E_s^d is the downstream signal, and E_s^u is the upstream signal. E_{RB}^d and E_{RB}^u are the Rayleigh backscattered signals of E_s^d and E_s^u , respectively.

4.3 System experiment for the symmetric bidirectional traffic by using 4-port interleaver

As internet traffic grows rapidly, it is desirable to increase the spectral efficiency of the wavelength division multiplexing (WDM) networks. Bidirectional transmission

is one of the effective ways in WDM networks to increase the bandwidth utilization and reduce operation cost. One of the core technologies in bidirectional transmission is bidirectional amplification, which requires high gain, low noise and removal of Rayleigh backscattering (RB). Typical implementation of bidirectional amplification is with appropriate band splitting or channel interleaving, or using a gain-clamping SOA, called linear optical amplifier (LOA). In the first scheme, either a pair of WDMs or circulators are needed to split up the east and west traffics and each traffic is individually amplified by a corresponding EDFA. The gains of EDFAs are typically limited to avoid the RB self-oscillation in this method. In the LOA scheme, because of the gain-clamping effect, the gain is limited to be less than 20-dB and high noise figure (NF) is inevitable.. Several types of bi-directional optical amplifiers (BOA) have been reported; two amplifiers with two direction-selective components, and one amplifier with four direction-selective components. These studies used two wavelength bands to suppress the transmission performance degradation caused by Rayleigh back-scattering (RB).

These will greatly reduce the amplification span and optical signal to noise ratio (OSNR), thus increase the operational cost and degrade the transmission quality. In this study, we proposed and experimentally demonstrated a novel four-port interleaver that enables bidirectional transmission using only unidirectional amplification. The primary functions of this four-port interleaver are to re-direct the east and west traffic into uni-direction and, in the mean time, provide simultaneous crosstalk and noise reduction.

4.3.1 Operation principle

The operating principle is done by the function of the four-port interleaver. The function of the interleaver is mentioned in the chapter 2. The interleaver we used is a symmetrical four-port interleaver with two input and two output ports. The detail

configuration is shown in Fig. 4.5.

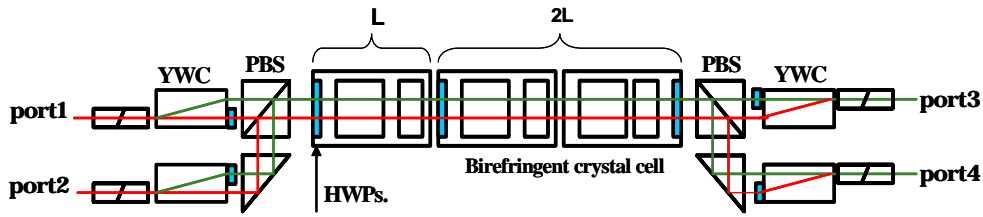


Fig. 4.5. Detail configuration of an L-2L interleaver

It incorporates the birefringent crystal cells; half wave plates (HWP), YVO4 walk off crystals (YWC) and polarization beam splitters (PBS). Fig. 4.6 illustrates the measured amplitude response of the interleaver for even and odd channels. The channel spacing of this interleaver is 50-GHz with insertion loss of 2.2-dB and 0.5-dB pass band of around 35-GHz, respectively.

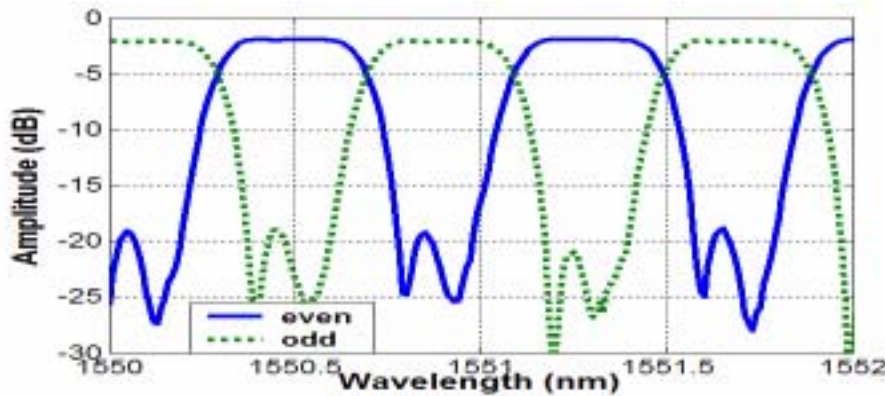


Fig. 4.6. pass band of the interleaver for even and odd channel

We design the interleaver to have complementary wavelength dependent routing characteristics. For example, if λ_1 (odd channel) enters port 1, it will be routed to port 4. However, when λ_2 (even channel) goes into port 2, it will also be directed to port 4. By using this interleaver property, when east-even channels arrive at port 2 of the interleaver, they will be sent to port 4. On the other hand, when the west-odd channels go into port 1 of the interleaver, they will be routed to port 4 as well. Therefore, we can re-route a bidirectional transmission into a unidirectional transmission and achieve unidirectional amplification with a single EDFA, as shown in Fig.4.7.

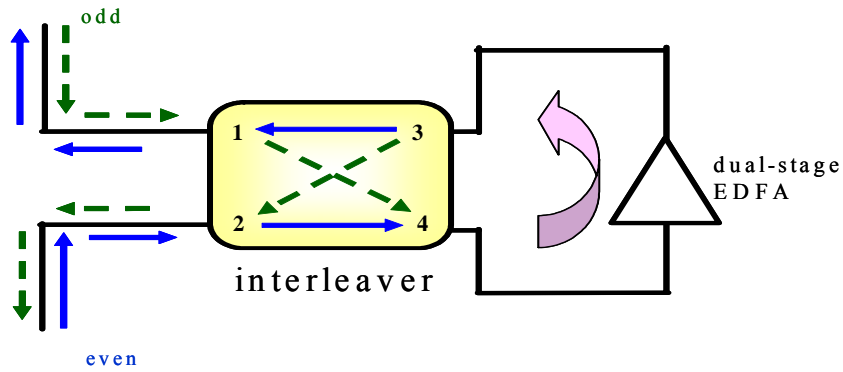


Fig. 4.7. The way of changing bidirectional transmission into unidirection by the interleaver.

4.3.2 Setup & Results

To demonstrate this novel wavelength sensitive routing characteristic of the four-port interleaver, we set up a bidirectional transmission system as illustrated in Fig. 4.9. We used a dual-stage EDFA with dispersion compensation mid-stage to provide the unidirectional loss and dispersion compensation. The eight channel laser sources consist of two groups: one from 1550.52-nm to 1551.72-nm and the other from 1554.54-nm to 1555.75-nm, all on the standard ITU 50-GHz channel spacing grids. Fig 4.8 shows the eye diagram of the input signal.

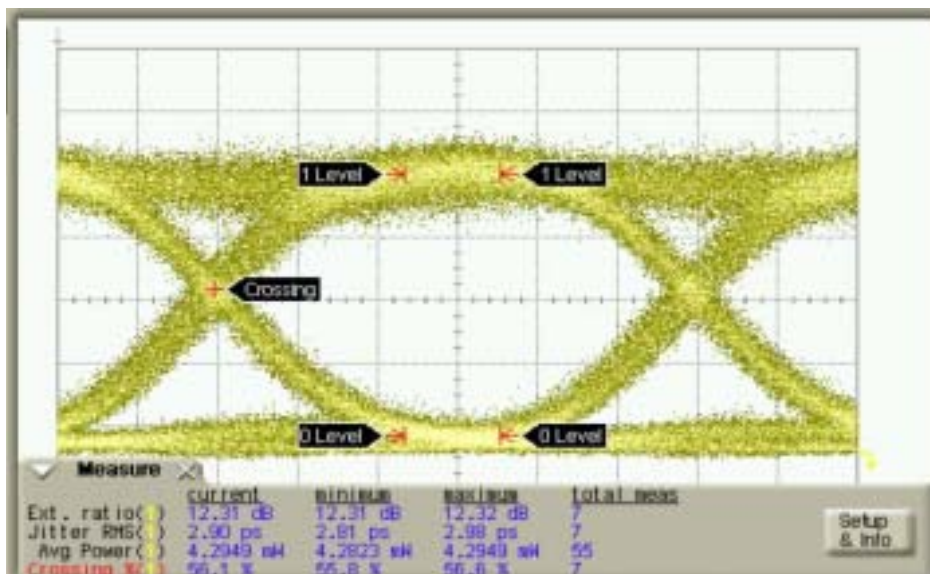


Fig. 4.8. The eye diagram of the input signal and corresponding parameters

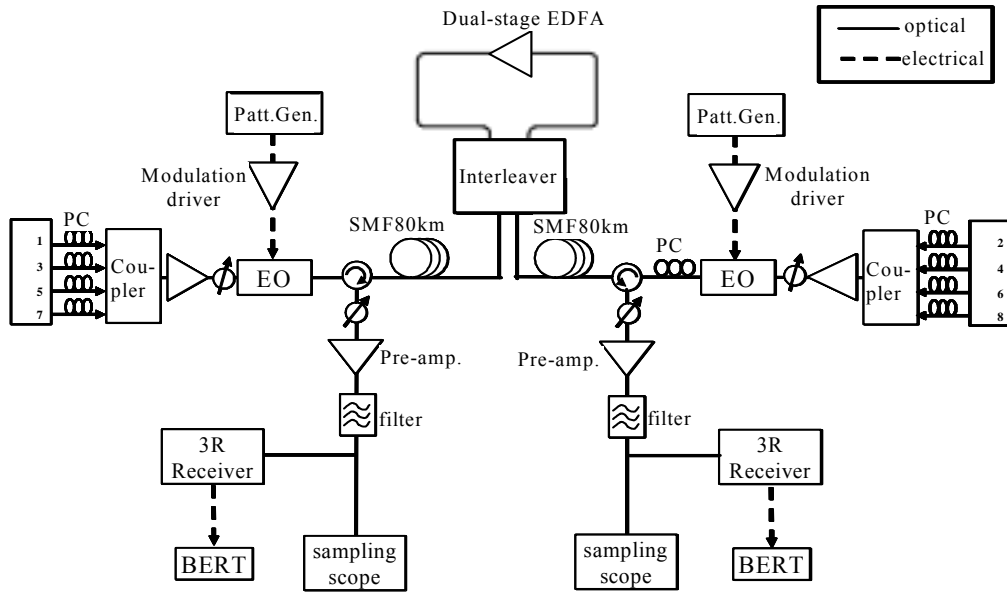


Fig. 4.9. Experimental setup of a bidirectional transmission

They were individually modulated by a LiNbO₃ electro-optical (EO) modulator at 10 Gb/s with a pseudo-random binary sequence (PRBS) length of $2^{31}-1$ pattern. The transmission fiber we used were 160-km of standard single mode fiber (Corning SMF-28[®]). Within the dual-stage EDFA, 31-km of Corning dispersion compensation fiber (DCF) was inserted to compensate the accumulated chromatic dispersion in 160-km of SMF fiber. A 3R receiver of -32 -dBm back-to-back sensitivity at bit error ratio (BER) of 10^{-9} was applied to evaluate the signal's performance after transmission. The gains and noise figures of our dual-stage EDFA at all channels are about 23.5-dB and 4.5-dB, respectively. Fig. 4.8 shows the received optical spectrum of the east-even channels after 160-km of transmission. Since we re-route the bidirectional transmission into unidirectional at the amplification stage using an interleaver, the noises are diminished significantly. The primary reflection path is showed in the figure 4.11. From this figure we could determine the suppression of the unwanted reflection signal at the receiver is dependent on the isolation of the interleaver. Consequently, the optical signals experience much lower NF, when compared with > 6.5 -dB of NF by using a LOA. Therefore, we can achieve OSNR of

exceeding 35-dB after 160-km of transmission at all channels in our proposed method, compared with those of < 26-dB of OSNR in. Fig. 4.12(a)~(h) illustrates the BER curves and the corresponding eye diagrams of each channel. After 160-km transmission, both eye diagrams and BER curves indicate that the performance degradation due to the accumulated ASE noise and dispersion in the bi- and uni-directional transmission systems was similar.

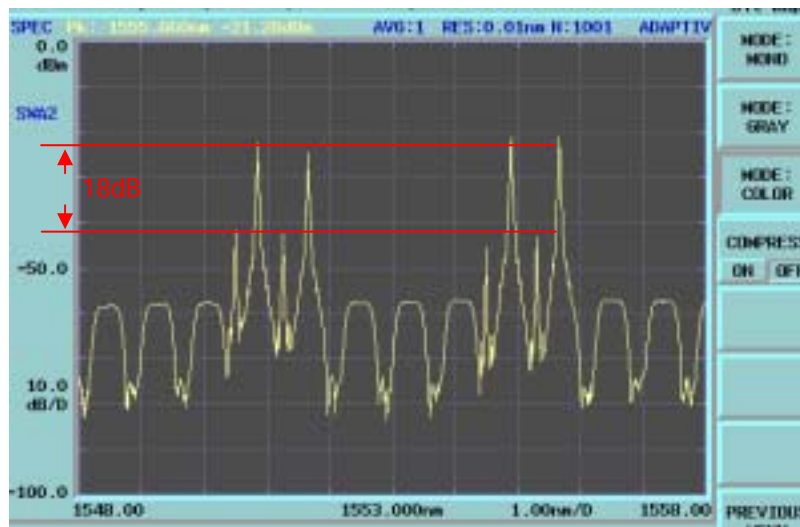


Fig. 4.10(a). Received optical spectrum of the east-even traffic after 160-km transmission

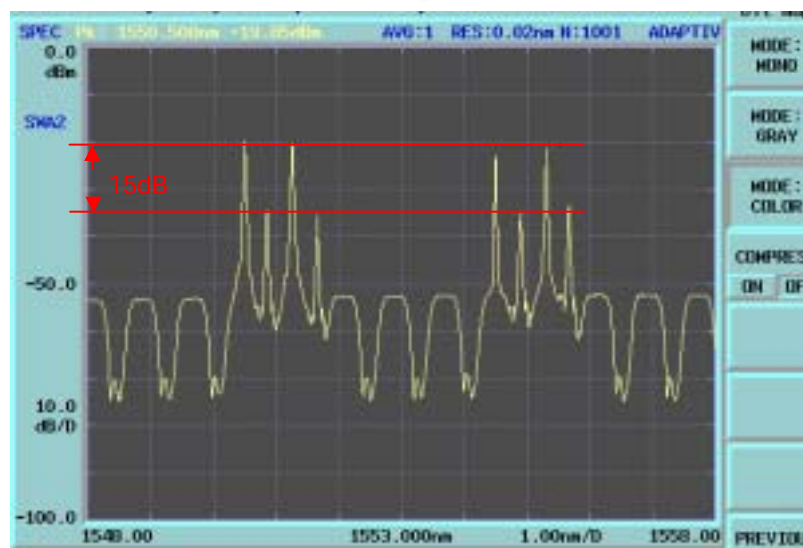


Fig. 4.10(b). Received optical spectrum of the west-odd traffic after 160-km transmission

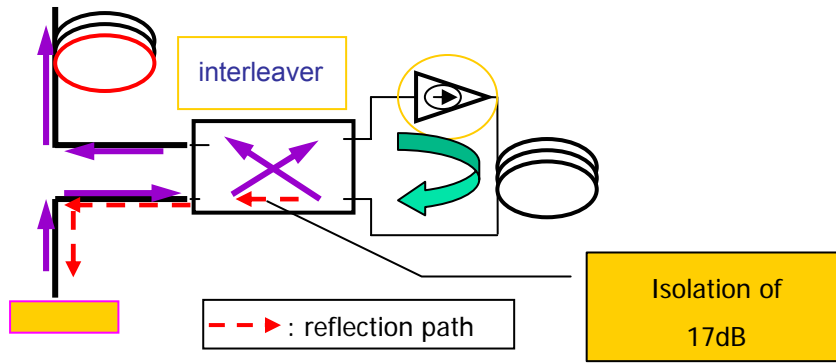


Fig. 4.11. primary reflection path

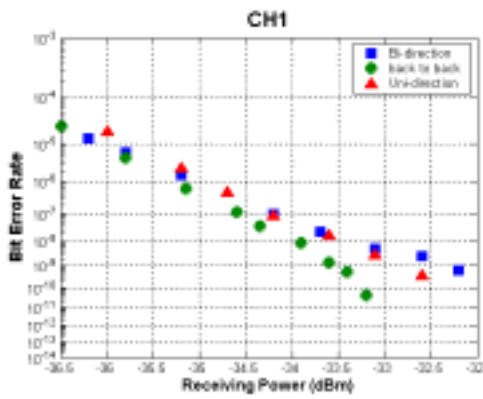


Fig. 4.12(a). BER curve for 160 km bidirectional transmission of channel 1

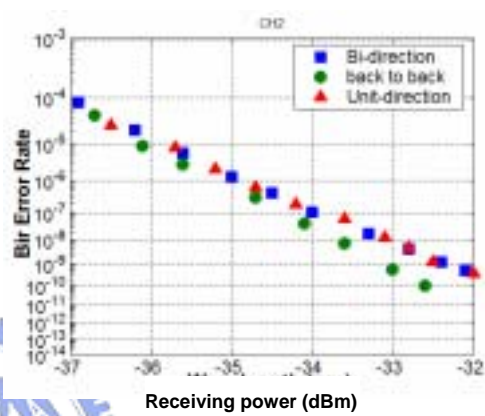


Fig. 4.12(b). BER curve for 160 km bidirectional transmission of channel 2

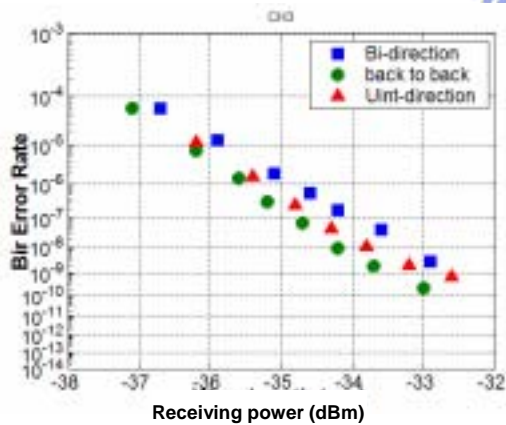


Fig. 4.12(c). BER curve for 160 km bidirectional transmission of channel 3

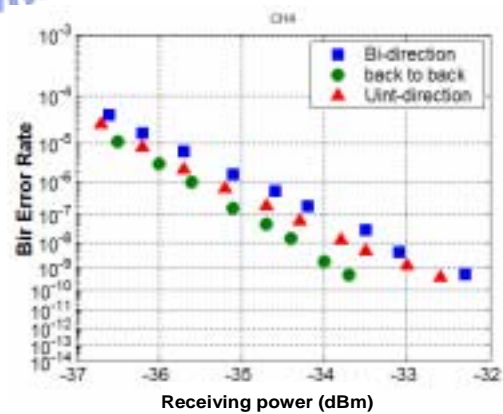


Fig. 4.12(d). BER curve for 160 km bidirectional transmission of channel 4

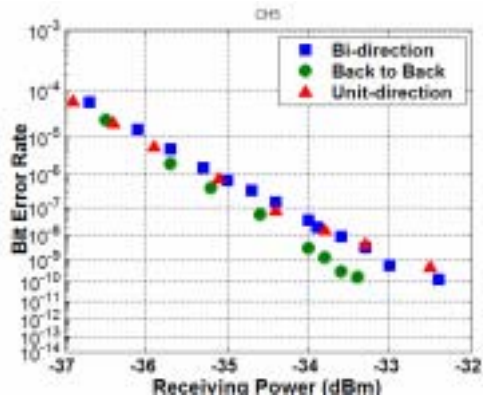


Fig. 4.12(e). BER curve for 160 km bidirectional transmission of channel 5

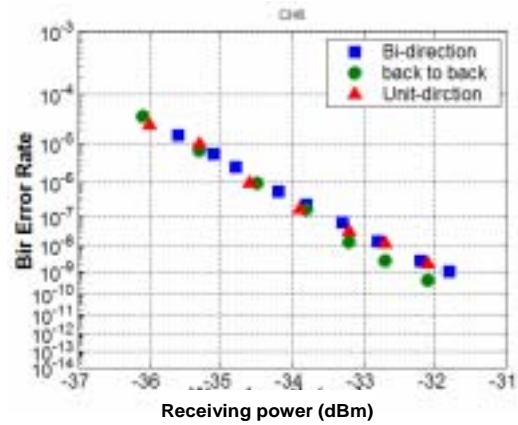


Fig. 4.12(f). BER curve for 160 km bidirectional transmission of channel 6

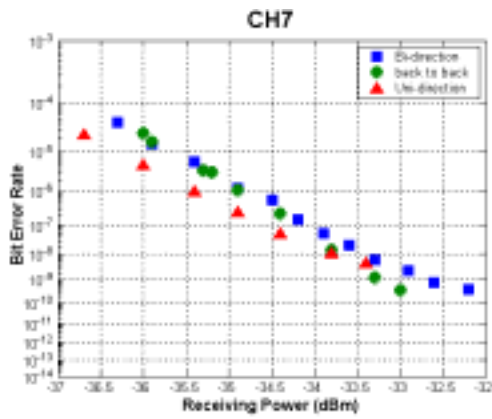


Fig. 4.12(e). BER curve for 160 km bidirectional transmission of channel 7

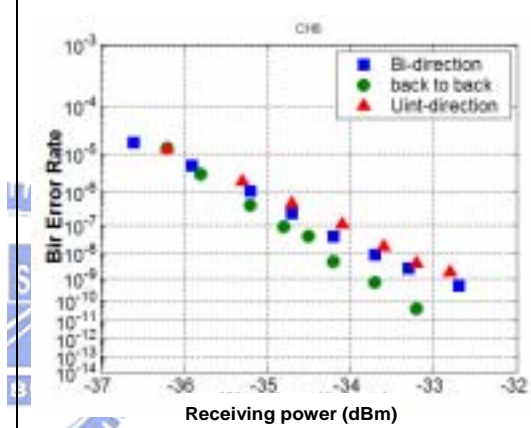


Fig. 4.12(f). BER curve for 160 km bidirectional transmission of channel 8

In addition, the power penalty of each channel is showed in figure 4.13. We also measure the noise figure and the net gain of our bidirectional amplifier module for each channel showed in figure 4.14.

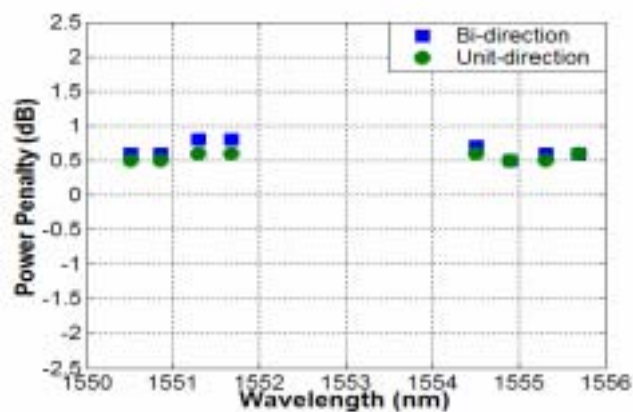


Fig. 4.13. Power penalty of each channel

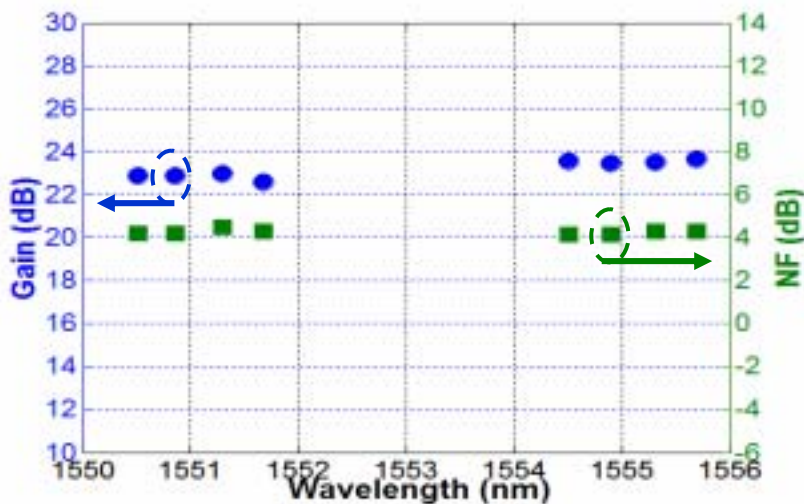


Fig. 4.14. Noise figure and net gain of the proposed bidirectional amplifier

Denote that all the penalties are less than 0.8 dB compared with back-to-back BER curve and as can be clearly seen from this figure, the BER penalty variations between bidirectional and unidirectional transmission are less than 0.2 dB at all channels. The maximum noise figure is less than 4.5 dB.

Furthermore, we extended the transmission length to 210 km and also applied the corresponding DCF to compensate the chromatic dispersion. As a result, the BER curve for each channel (figure 4.15 (a) ~ (h)) including of the corresponding power penalty (figure 4.16), noise and net gain of the bidirectional amplifier figure (figure 4.17) are measured as below.

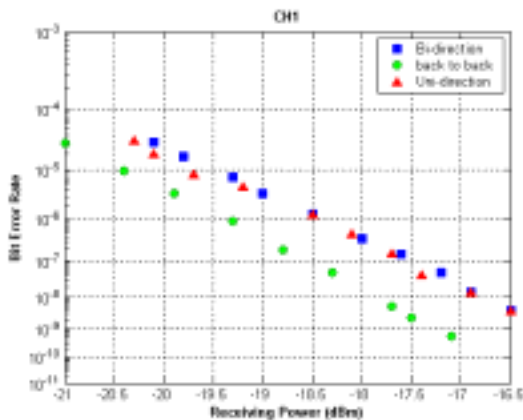


Fig. 4.15(a). BER curve for 210 km bidirectional transmission of channel 1

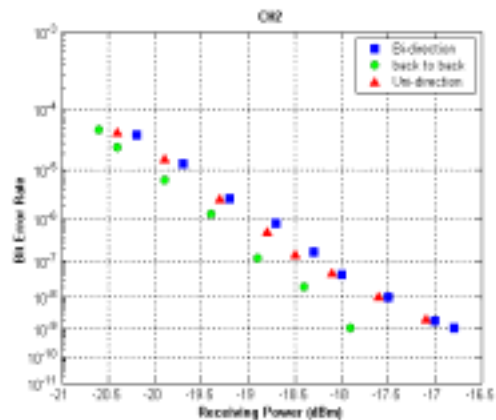


Fig. 4.5(b). BER curve for 210 km bidirectional transmission of channel 2

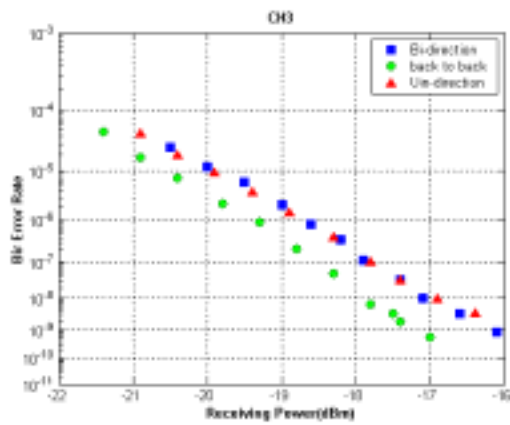


Fig. 4.15(c). BER curve for 210 km bidirectional transmission of channel 3

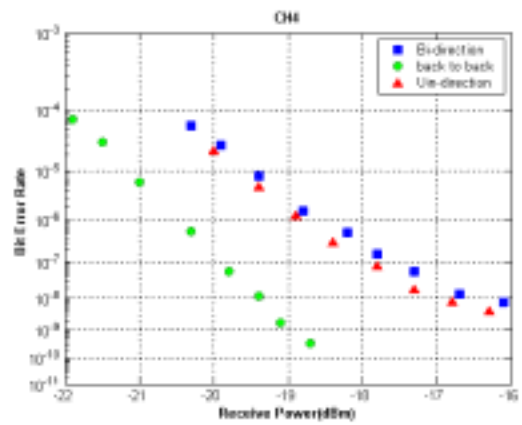


Fig. 4.15(d). BER curve for 210 km bidirectional transmission of channel 4

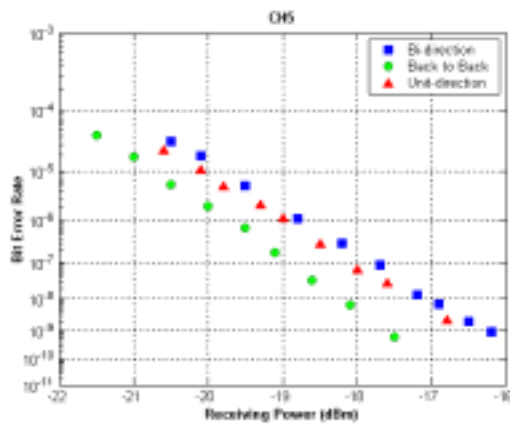


Fig. 4.15(e). BER curve for 210 km bidirectional transmission of channel 5

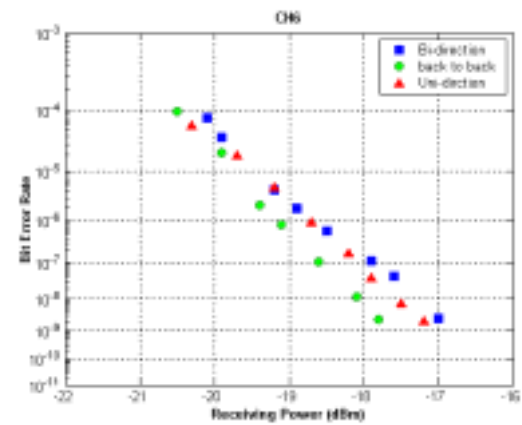


Fig. 4.15(f). BER curve for 210 km bidirectional transmission of channel 6

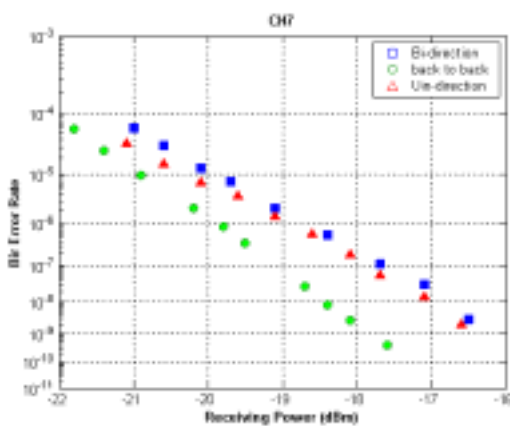


Fig. 4.15(g). BER curve for 210 km bidirectional transmission of channel 7

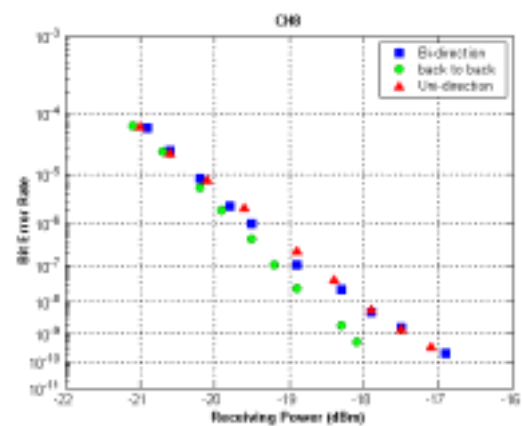


Fig. 4.15(h). BER curve for 210 km bidirectional transmission of channel 8

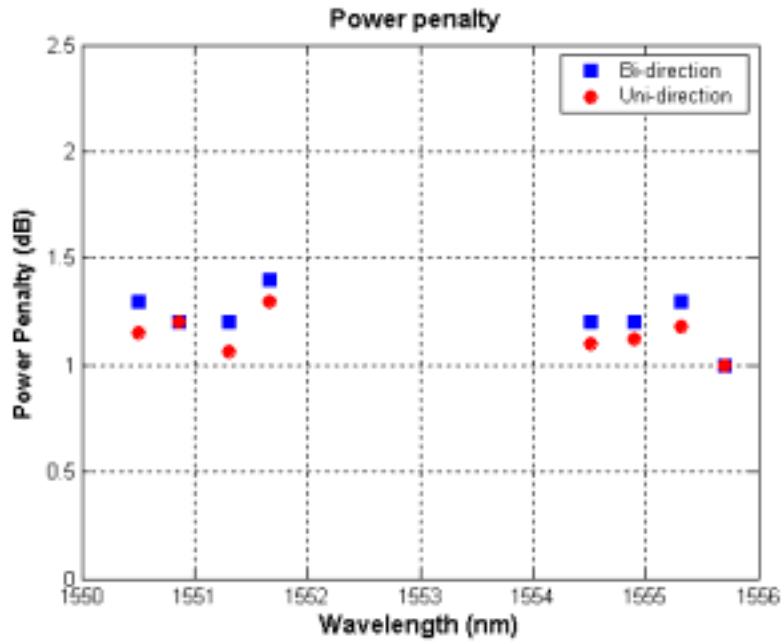


Fig. 4.16. Power penalty of each channel for 210km transmission

Denote that the maximum power penalty compared with back to back transmission is less than 1.5 dB.

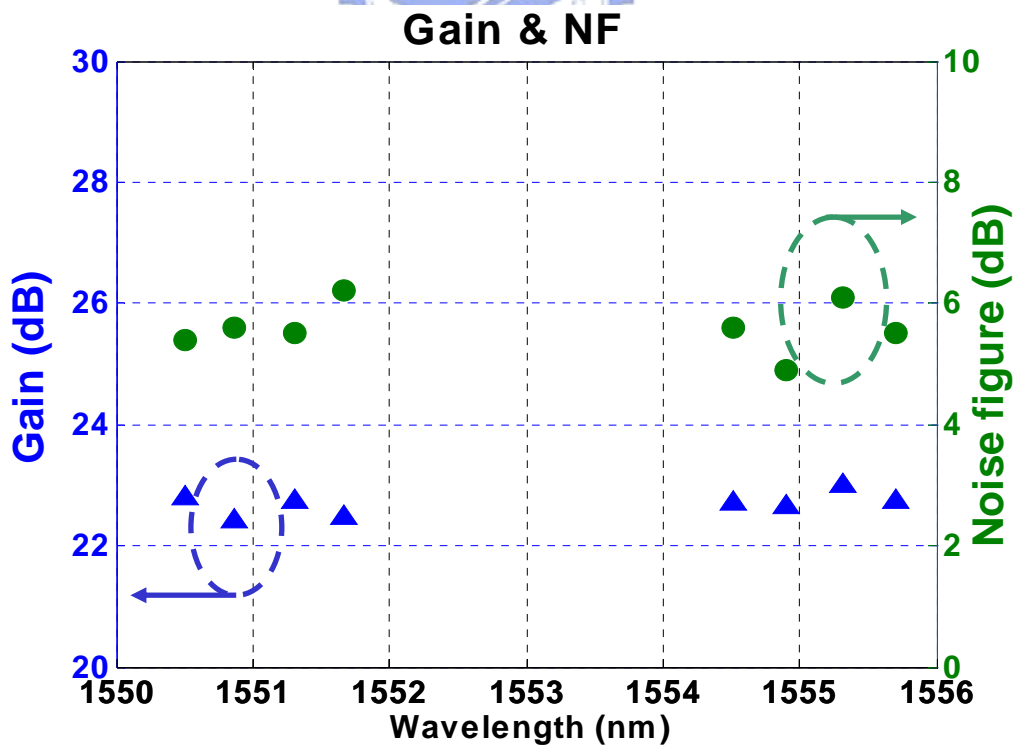


Fig. 4.17 Net gain and noise figure of each channel for 210km transmission

Denote the net gain for each channel is about 22.2 ~23dB and the noise figure is

about 6 dB.

In order to investigate the limit of reflection suppression, we also measure the transmission characteristics of the circulator we used, showed in figure 4.18. As a result, the optical spectrum before the receiver is showed in figure 4.19. We found that the primary limiting the suppression of the unwanted reflection noise is the isolation of the circulator before the receiver.

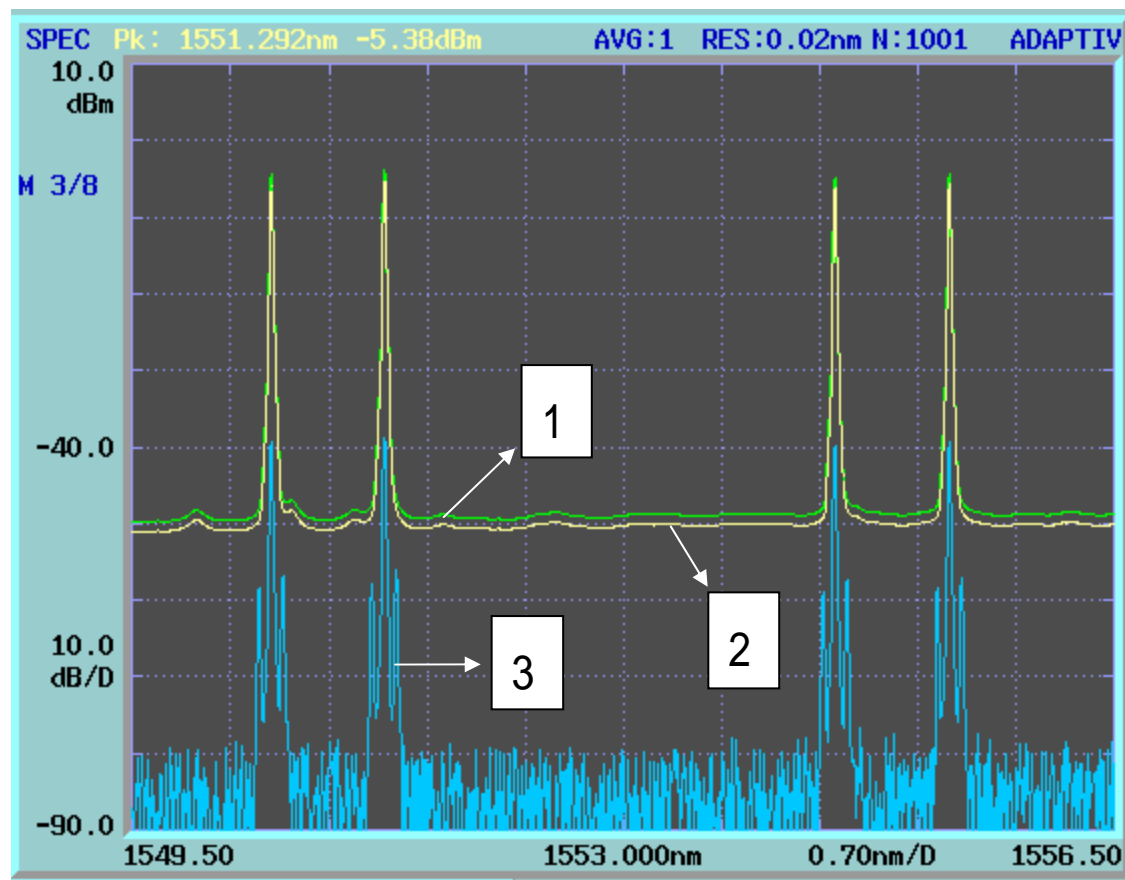
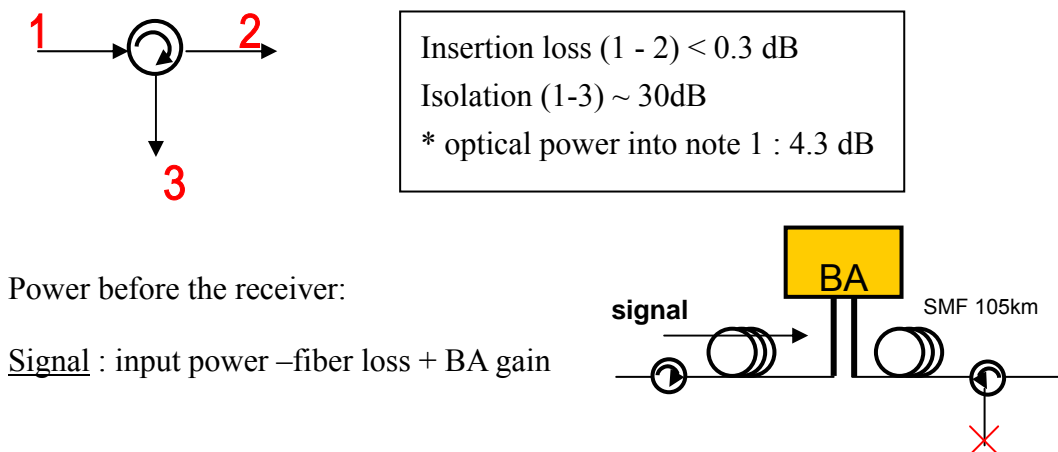


Fig. 4.18. Transmission characteristics of the circulator



interference 1 : input power -30 dB isolation (circulator)

interference 2 : input power –fiber loss + BA gain -17dB isolation (interleaver)

→ Suppression of reflection ~ (-fiber loss + BA gain)- (-30 dB) ~ **10 dB**

We achieve very good agreement from the optical spectrum measured before the receiver.

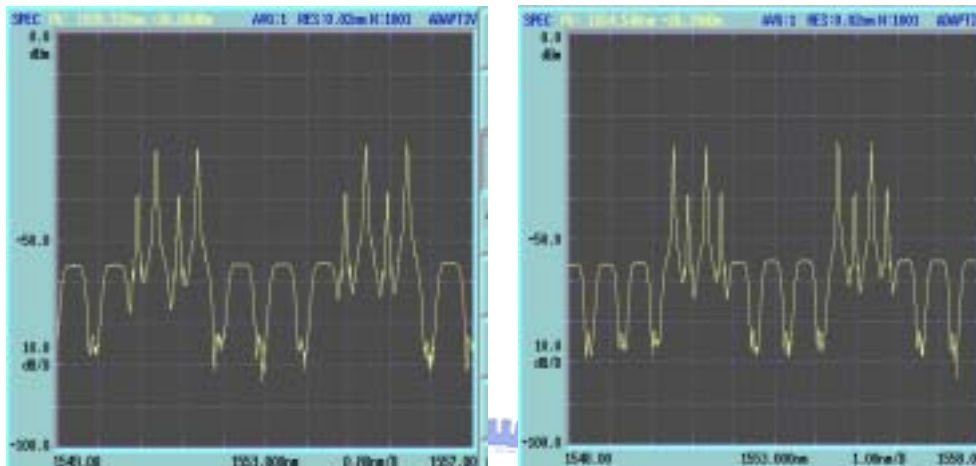


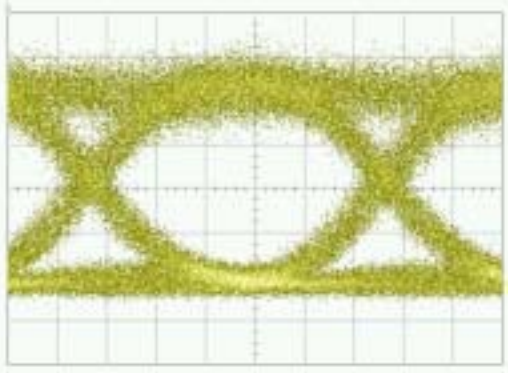
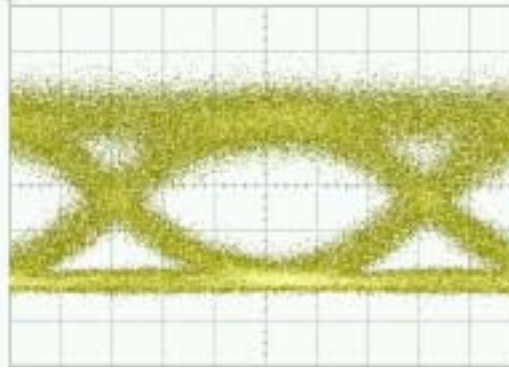
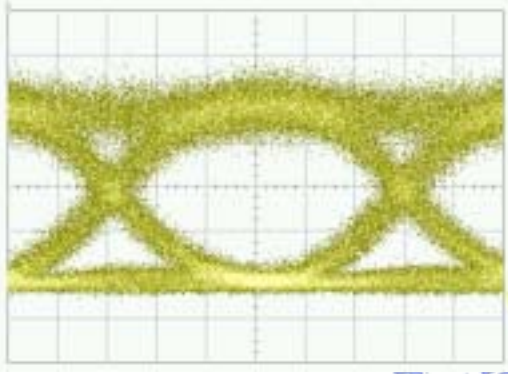
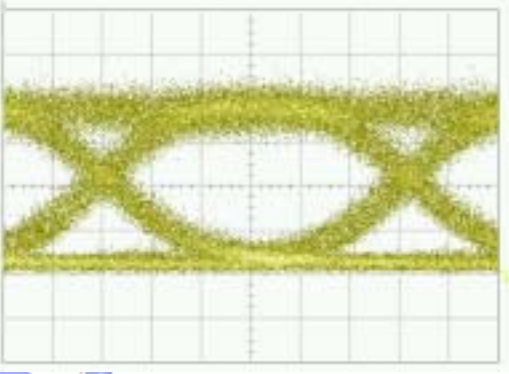
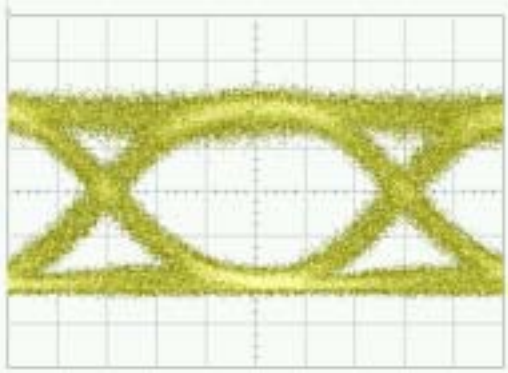
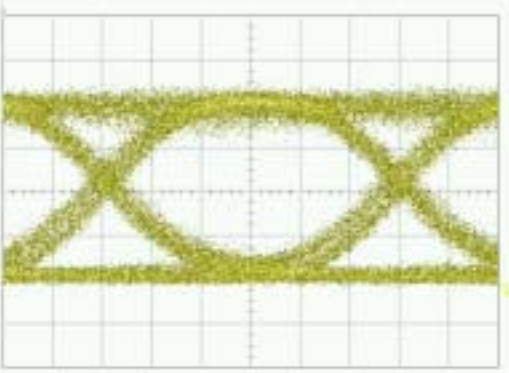
Fig. 4.19. Optical spectrum before the receiver

From the figure above, some comparison between 160 km and 210 km SMF transmission could be made as below:

	160km	210km
Sensitivity penalty	0.6~ 0.8dB	1~1.4dB
OSNR penalty	~2.1 dB	~2.1 dB
Gain	23 dB	23 dB
Noise Figure	4.5dB	5.6dB

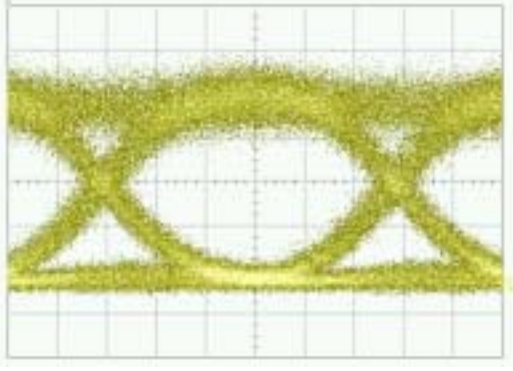
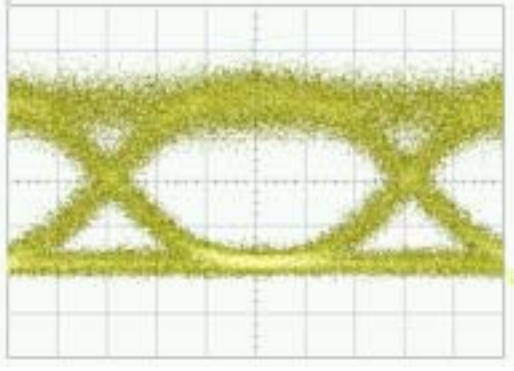
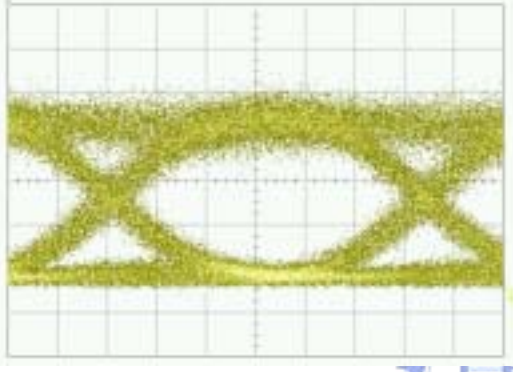
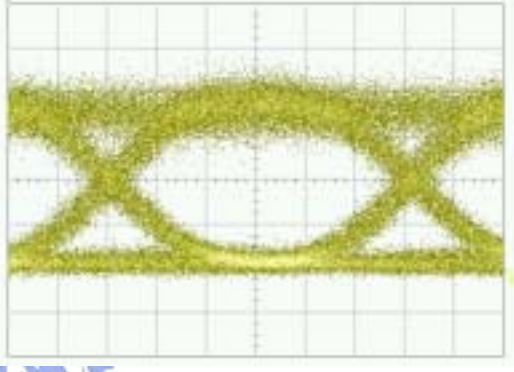
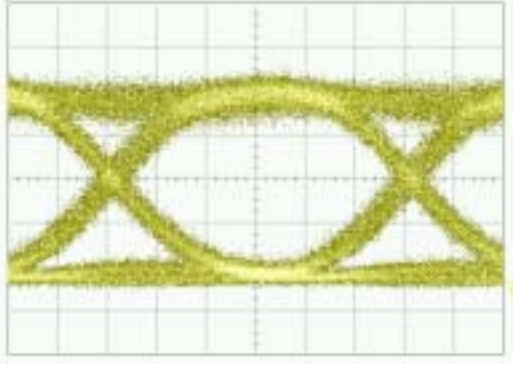
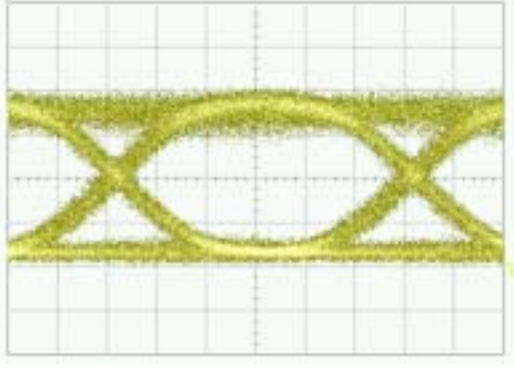
The eye diagrams for 160km and 210km SMF transmission (including of the bidirectional, unidirectional and back to back transmission) are measure in figure 4.20

(a)~(h) and figure 4.21 (a)~(h), respectively

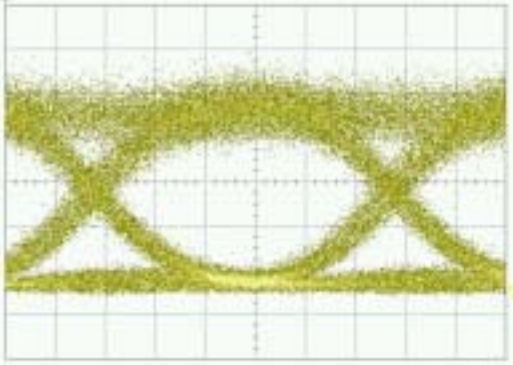
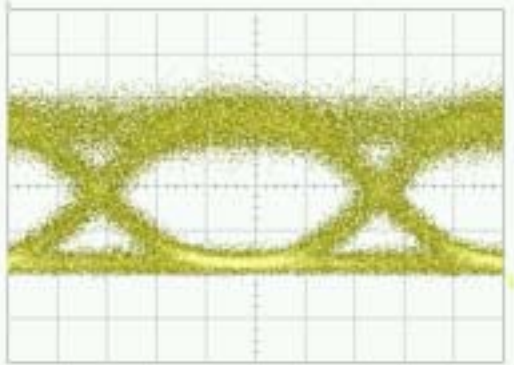
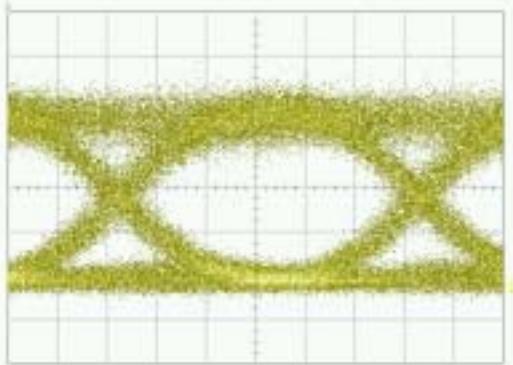
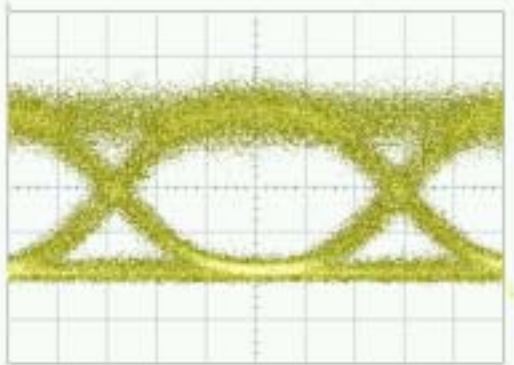
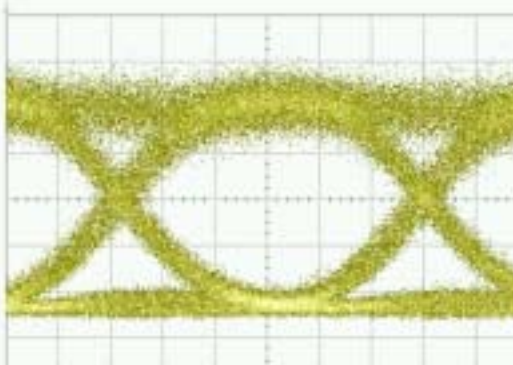
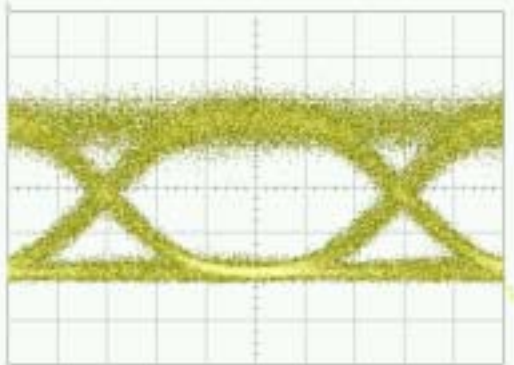
	
Fig. 4.20(a)-1. Eye diagram for 160 km transmission of channel 1 (bi-directional)	Fig. 4.21(a)-1. Eye diagram for 210 km transmission of channel 1 (bi-directional)
	
Fig. 4.20(a)-2. Eye diagram for 160 km transmission of channel 1 (uni-directional)	Fig. 4.21(a)-2. Eye diagram for 210 km transmission of channel 1 (uni-directional)
	
Fig.4.20(a)-3. Eye diagram for 160 km transmission of channel 1 (back to back)	Fig. 4.21(a)-3. Eye diagram for 210 km transmission of channel 1 (back to back)

<p>Fig. 4.20(b)-1. Eye diagram for 160 km transmission of channel 2 (bi-directional)</p>	<p>Fig. 4.21(b)-1. Eye diagram for 210 km transmission of channel 2 (bi-directional)</p>
<p>Fig. 4.20(b)-2. Eye diagram for 160 km transmission of channel 2 (uni-directional)</p>	<p>Fig. 4.21(b)-2. Eye diagram for 210 km transmission of channel 2 (uni-directional)</p>
<p>Fig. 4.20(b)-3. Eye diagram for 160 km transmission of channel 2 (back to back)</p>	<p>Fig. 4.21(b)-3. Eye diagram for 210 km transmission of channel 2 (back to back)</p>

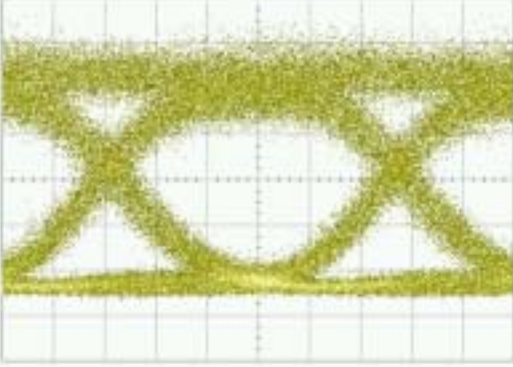
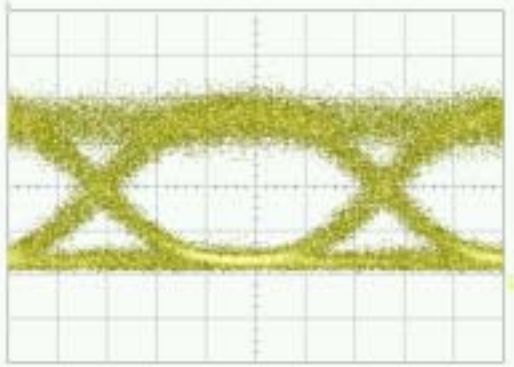
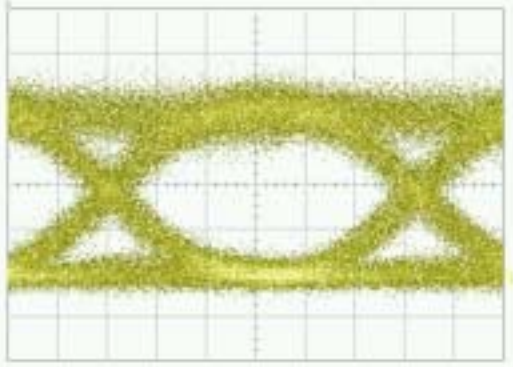
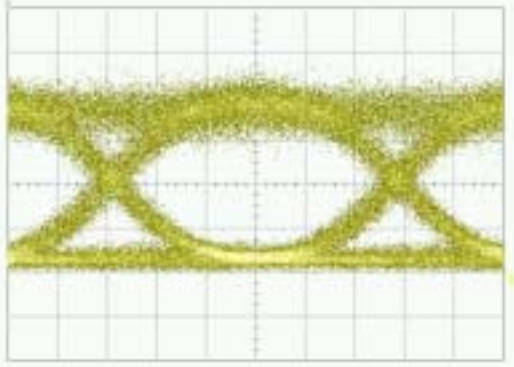
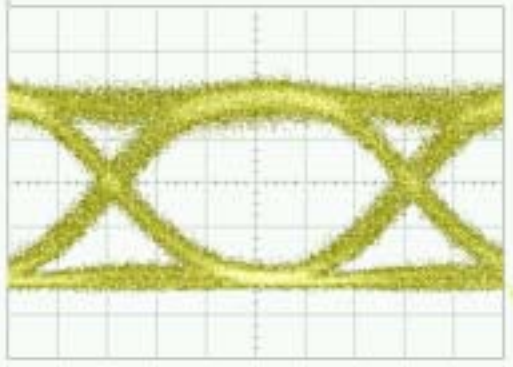
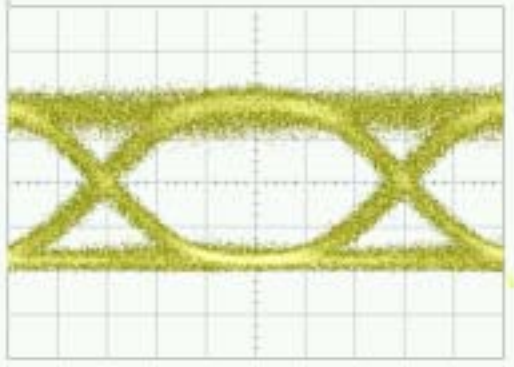
<p>Fig. 4.20(c)-1. Eye diagram for 160 km transmission of channel 3 (bi-directional)</p>	<p>Fig. 4.21(c)-1. Eye diagram for 210 km transmission of channel 3 (bi-directional)</p>
<p>Fig. 4.20(c)-2. Eye diagram for 160 km transmission of channel 3 (uni-directional)</p>	<p>Fig. 4.21(c)-2. Eye diagram for 210 km transmission of channel 3 (uni-directional)</p>
<p>Fig. 4.20(c)-3. Eye diagram for 160 km transmission of channel 3 (back to back)</p>	<p>Fig. 4.21(c)-3. Eye diagram for 210 km transmission of channel 3 (back to back)</p>

	
<p>Fig. 4.20(d)-1. Eye diagram for 160 km transmission of channel 4 (bi-directional)</p>	<p>Fig. 4.21(d)-1. Eye diagram for 210 km transmission of channel 4 (bi-directional)</p>
	
<p>Fig. 4.20(d)-2. Eye diagram for 160 km transmission of channel 4 (uni-directional)</p>	<p>Fig. 4.21(d)-2. Eye diagram for 210 km transmission of channel 4 (uni-directional)</p>
	
<p>Fig. 4.20(d)-3. Eye diagram for 160 km transmission of channel 4 (back to back)</p>	<p>Fig.4.21(d)-3. Eye diagram for 210 km transmission of channel 4 (back to back)</p>

<p>Fig. 4.20(e)-1. Eye diagram for 160 km transmission of channel 5 (bi-directional)</p>	<p>Fig. 4.21(e)-1. Eye diagram for 210 km transmission of channel 5 (bi-directional)</p>
<p>Fig. 4.20(e)-2. Eye diagram for 160 km transmission of channel 5 (uni-directional)</p>	<p>Fig. 4.21(e)-2. Eye diagram for 210 km transmission of channel 5 (uni-directional)</p>
<p>Fig. 4.20(e)-3. Eye diagram for 160 km transmission of channel 5 (back to back)</p>	<p>Fig. 4.21(e)-3. Eye diagram for 210 km transmission of channel 5 (back to back)</p>

	
<p>Fig. 4.20(f)-1. Eye diagram for 160 km transmission of channel 6 (bi-directional)</p>	<p>Fig. 4.21(f)-1. Eye diagram for 210 km transmission of channel 6 (bi-directional)</p>
	
<p>Fig. 4.20(f)-2. Eye diagram for 160 km transmission of channel 6 (uni-directional)</p>	<p>Fig. 4.21(f)-2. Eye diagram for 210 km transmission of channel 6 (uni-directional)</p>
	
<p>Fig. 4.20(f)-3. Eye diagram for 160 km transmission of channel 6 (back to back)</p>	<p>Fig. 4.21(f)-3. Eye diagram for 210 km transmission of channel 6 (back to back)</p>

<p>Fig. 4.20(g)-1. Eye diagram for 160 km transmission of channel 7 (bi-directional)</p>	<p>Fig. 4.21(g)-1. Eye diagram for 210 km transmission of channel 7 (bi-directional)</p>
<p>Fig. 4.20(g)-2. Eye diagram for 160 km transmission of channel 7 (uni-directional)</p>	<p>Fig. 4.21(g)-2. Eye diagram for 210 km transmission of channel 7 (uni-directional)</p>
<p>Fig. 4.20(g)-3. Eye diagram for 160 km transmission of channel 7 (back to back)</p>	<p>Fig. 4.21(g)-3. Eye diagram for 210 km transmission of channel 7 (back to back)</p>

	
<p>Fig. 4.20(h)-1. Eye diagram for 160 km transmission of channel 8 (bi-directional)</p>	<p>Fig. 4.21(h)-1. Eye diagram for 210 km transmission of channel 8 (bi-directional)</p>
	
<p>Fig. 4.20(h)-2. Eye diagram for 160 km transmission of channel 8 (uni-directional)</p>	<p>Fig. 4.21(h)-2. Eye diagram for 210 km transmission of channel 8 (uni-directional)</p>
	
<p>Fig. 4.20(h)-3. Eye diagram for 160 km transmission of channel 8 (back to back)</p>	<p>Fig. 4.21(h)-3. Eye diagram for 210 km transmission of channel 8 (back to back)</p>

Clearly, there is no obvious pulse distortion observed from the eye diagrams.

References

- [3.1] C. H. Kim, Chang-Hee Lee, and Y. C. Chung, Member, IEEE, A Novel Bidirectional Add/Drop Amplifier (BADA), IEEE PHOTONICS TECHNOLOGY LETTERS, VOL. 10, NO. 8, AUGUST 1998
- [3.2] S.-K. Liaw, K.-P. Ho, C. Lin, and S. Chi, "Multichannel bidirectional transmission using a WDM MUX/DMUX pair and unidirectional in-line amplifiers," *IEEE Photon. Technol. Lett.*, vol. 9, no. Dec., pp. 1664–1666, 1997.
- [3.3] M. Oskar van Deventer, Jos J. G. M van der To1 and Andrk J. Boot, Power Penalties Due to Brillouin and Rayleigh Scattering in a Bidirectional Coherent Transmission System, IEEE PHOTONICS TECHNOLOGY LE'ITERS, VOL. 6, NO. 2, FEBRUARY 1994
- [3.4] Jang-won Park and Chang-Hee Lee, Wavelength interleaved bidirectional add/drop amplifier module, IEEE PHOTONICS TECHNOLOGY LETTERS, VOL. 12, NO. 2, FERBRUARY 2002.
- [3.5]Jeongyun Ko, Seongha Kim, Jaehoon Lee, Shinhee Won, Y.S kim, and Jichai Jeong, Estimation of Performance Degradation of Bidirectional WDM Transmission Systems Due to Rayleigh Backscattering and ASE Noise Using Numerical and Analytical models, journal of lightwave technology, vol.21, no. 4, april 2003
- [3.6] Seung-Tak Lee and Chang-Joon Chae, Member, IEEE, Low-Cost Bidirectional Optical Amplifier Using a Unidirectional Er-Doped Fiber Amplifier and a Fiber Mach–Zehnder Interferometer, IEEE PHOTONICS TECHNOLOGY LETTERS, VOL. 13, NO. 1, JANUARY 2001.

Chapter 5

Conclusions

The original design separates (or combines) even channels from odd channels across a DWDM comb. According to the filtering characteristics, there are many applications could be made. Finally, we successfully demonstrated two system experiments by using four-port interleaver.

In the first experiment, the investigation presents a cascability study of a 50-GHz channel spacing dispersion-compensated interleaver pair using a re-circulating loop. After five cascaded nodes and 525 km of transmission, the interleaver-induced dispersion did not significantly degrade the system performance when wavelengths were exactly aligned to ITU grids. However, when the wavelength deviated from ITU grids, the sensitivity variation of the compensated case was much less than that of the uncompensated pair.

Experimental results show that, with 10-GHz wavelength detuning, the sensitivity variations of these two configurations are less than 0.4 dB and more than 2.5 dB, for compensated and uncompensated cases, respectively. Such results can lessen the precision requirements in selecting DFB lasers for metro add-drop network applications.

Next, we construct a bidirectional transmission system. By choosing channel frequency appropriately, the 4-port interleaver could be treated as a switch between bidirectional and unidirectional transmission. We proposed and experimentally demonstrated a novel four-port interleaver that enables bidirectional transmission using unidirectional amplification. Due to the innovative complementary wavelength sensitive routing scheme, using a single dual-stage EDFA, we achieve 160-km & 210-km bidirectional transmission with less than 0.2-dB sensitivity penalty variations

between bi- and uni-directional transmissions. In addition, the maximum power penalty compared to the back to back transmission for 160 km and 210 km are 0.8 dB and 1.4 dB, respectively. The maximum gain is no longer limited by the Rayleigh backscattering. The net gain and noise figure of the proposed interleaver-based amplifier for bidirectional transmission is about 23 dB and 5.6dB for 210km, respectively. .

